Abrupt transitions in the NAO control of explosive North Atlantic cyclone development

Iñigo Gómara[1,2*], Belén Rodríguez-Fonseca[1,2], Pablo Zurita-Gotor[1,2], Sven Ulbrich[3], and Joaquim G. Pinto[3,4]

Running Title: Non-stationary variability of North Atlantic bombs

[1] *Dpto. Geofísica y Meteorología, Universidad Complutense de Madrid, Madrid, Spain*

[2] *Instituto de Geociencias (IGEO), UCM, CSIC, Madrid, Spain*

[3] *Institute for Geophysics and Meteorology, University of Cologne, Cologne, Germany*

[4] *Department of Meteorology, University of Reading, Reading, United Kingdom*

Submitted to

Climate Dynamics

26 June 2015

Revised on 22 January 2016

Accepted on 26 January 2016

[*]**Correspondence to:** Iñigo Gómara, Dpto. Geofísica y Meteorología, Universidad Complutense de Madrid, Facultad de CC. Físicas, Ciudad Universitaria s/n. 28040 Madrid, Spain. E-mail: i.gomara@ucm.es

Abstract

Explosive cyclones are intense extra-tropical low pressure systems featuring large deepening rates. In the Euro-Atlantic sector, they are a major source of life-threatening weather impacts due to their associated strong wind gusts, heavy precipitation and storm surges. The wintertime variability of the North Atlantic cyclonic activity is primarily modulated by the North Atlantic Oscillation (NAO). In this study, we investigate the interannual and multi-decadal variability of explosive North Atlantic cyclones using track density data from two reanalysis datasets (NCEP and ERA-40) and a control simulation of an atmosphere/ocean coupled General Circulation Model (GCM - ECHAM5/MPIOM1). The leading interannual and multi-decadal modes of variability of explosive cyclone track density are characterized by a strengthening/weakening pattern between Newfoundland and Iceland, which is mainly modulated by the NAO at both timescales. However, the NAO control of interannual cyclone variability is not stationary in time and abruptly fluctuates during periods of 20-25 years long both in NCEP and ECHAM5/MPIOM1. These transitions are accompanied by structural changes in the leading mode of explosive cyclone variability, and by decreased/enhanced baroclinicity over the sub-polar/sub-tropical North Atlantic. The influence of the ocean is apparently important for both the occurrence and persistence of such anomalous periods. In the GCM, the Atlantic Meridional Overturning Circulation (AMOC) appears to influence the large-scale baroclinicity and explosive cyclone development over the North Atlantic. These results permit a better understanding of explosive cyclogenesis variability at different climatic timescales and might help to improve predictions of these hazardous events.

Keywords: extra-tropical cyclones; explosive cyclogenesis; NAO; jet stream; ocean variability; AMOC.

1. Introduction

The wintertime variability in the mid-latitudes of both hemispheres is dominated by the occurrence of sub-weekly baroclinic disturbances (Blackmon et al. 1977; Lau 1978). Such disturbances typically grow in the vicinity of the planetary stationary troughs, where the gradients of temperature and humidity are maximum (Hoskins and Valdes 1990), and terminate near the regions of stationary ridges (Lau 1988). In the northern hemisphere, these areas (so called 'storm tracks') extend from the Eastern Asian and North American coast lines towards Western North America and Europe, respectively (Hoskins and Valdes 1990). In both oceanic basins, the storm track maximum lies northeast of the upper-level polar jet stream core, which is semi-permanently located over Japan and eastern North America, respectively (Chang and Orlanski 1993; Woollings et al. 2010). Such a configuration is consistent with surface baroclinic disturbances crossing the jet core from the right-entrance toward the left-exit regions, where strong upward motion of air fosters further cyclone amplification (Uccellini 1990; Rivière and Joly 2006). Additionally, upper-level mobile troughs (Bosart and Lin 1984; Sanders 1986; Reader and Moore 1995; Gyakum and Danielson 2000), and surface sensible and latent heat fluxes (Fosdick and Smith 1991; Davis and Emanuel 1988) also contribute to extra-tropical cyclone intensification. The characteristics of these dynamical precursors and their relative vertical position (Hoskins et al. 1985) typically determine the deepening rate (Pettersen and Smebye 1971; Fink et al. 2012) and life cycle of cyclones (Bjerknes and Solberg 1922; Shapiro and Keyser 1990). In the literature, surface cyclones featuring strong intensification rates (equal or above 24 hPa day^{-1} at 60˚N, or equivalent) are denominated 'explosive cyclones' or 'bombs' (Sanders and Gyakum 1980). These explosive cyclones are associated with strong impacts like wind gusts, heavy precipitation and storm surge events (Bosart and Lin 1984; Wernli et al. 2002).

Over the North Atlantic, the most prominent pattern of climate variability is the North Atlantic Oscillation (hereafter NAO; cf. Wanner et al. 2001). It represents a redistribution of air masses between sub-tropical and sub-polar latitudes, and modulates the strength and latitudinal location of the westerly flow (Marshall et al. 2001). Under its positive phase, the polar jet stream is accelerated and shifted to the northeast compared with its 'average' position. Under the negative phase, the jet stream is decelerated, constrained upstream in the North Atlantic and shifted to the south. The changed mean flow induces a latitudinal displacement of storm trajectories (Hurrell et al. 2003; Trigo 2006; Santos et al. 2013), and modulates their intensification rates (Gómara et al. 2014b). In this regard, the positive NAO phase is associated with stronger and more extensive baroclinicity over the North Atlantic than the negative phase. As a result, the number of intense cyclones over the North Atlantic increases (decreases) under NAO+ (NAO-) (Pinto et al. 2009).

The synoptic temporal evolution of the NAO seems to be dominated by stochastic processes (Feldstein 2003), such as Rossby Wave-Breaking (RWB; Benedict et al. 2004; Woollings et al. 2008; Strong and Magnusdottir 2008). RWB appears to control explosive cyclogenesis (Hanley and Caballero 2012; Gómara et al. 2014a; Messori and Caballero 2015) and cyclone families over Western Europe (Pinto et al. 2014) at synoptic timescales, by constraining and accelerating the jet. It has been debated in the literature whether the lower-frequency NAO variability (e.g., interannual, multi-decadal; James and James 1989; Wunsch 1999; Schneider et al. 2003; Raible et al. 2005) arises from pure climate noise (Stephenson et al. 2000), or is forced by external factors such as: (i) the interannual and lower frequency ocean variability in the North Atlantic (Raible et al. 2001; Visbeck et al. 2003; Rodríguez-Fonseca et al. 2006; Chen et al. 2015; Sun et al. 2015), tropical Pacific (Trenberth et al. 1998; Müller et al. 2008; Zhang et al. 2015) and the Indian ocean (Hoerling et al. 2001; 2004); (ii) the stratosphere (Baldwin and Dunkerton 2001; Reichler et al. 2012); (iii) solar variability (Shindell et al. 2001); and (iv) the mid-latitude westerly flow from the North Pacific (Honda et al. 2001; Pinto et al. 2011; Drouard et al. 2015), among others. Additionally, the role of anthropogenic climate change is another factor to consider. For example, there is some evidence of an intensification and eastward shift of the NAO dipole over the last decades of the 20th century (Hurrell et al. 2003; Jung et al. 2003). However, it is still unclear whether such evolution is primarily due to global warming (Ulbrich and Christoph 1999; Osborn et al. 1999; Bader et al. 2011), internal decadal variability of the NAO (Wang et al. 2012; Raible et al. 2014; Woollings et al. 2015) or to the storm track itself (Rogers 1997; Lu and Greatbach 2002).

Previous studies have characterized multi-decadal changes in the dominant teleconnection patterns, such as NAO, and their associated impacts, e.g., on European precipitation (Raible et al. 2004; Vicente-Serrano and López-Moreno 2008), on the North Atlantic storm track (Luksch et al. 2005, Pinto et al. 2011), etc. Such low-frequency changes often lead to active/inactive teleconnections between remote regions (e.g., between ENSO and European precipitation; López-Parages and Rodríguez-Fonseca 2012), thus providing enhanced forecast skill of relevant phenomena during specific periods of time (cf. Rodríguez-Fonseca et al. 2009; Losada et al. 2012).

This work primarily investigates the interannual variability of explosive cyclogenesis in the North Atlantic and its main potential drivers. Our focus is on the impact of the dominant modes of large-scale atmospheric variability (fundamentally NAO) and on the possible existence of different regimes of behavior as these modes and their associated teleconnections evolve in multi-decadal timescales. In addition, the multi-decadal variability of explosive cyclone tracks is also assessed. To address these questions, we use cyclone track density

fields obtained from reanalyses and a long coupled model simulation with an objective cyclone tracking algorithm.

The article is organized as follows. Sections 2 and 3 present the data and methods used in this study. Section 4 describes the explosive cyclone variability and its large-scale driving in the reanalysis data sets, and section 5 extends this analysis using a long control simulation from a coupled model. The article concludes with a short summary of the main results.

2. Data

Both reanalysis and GCM data are considered for this study. The first reanalysis dataset is provided by the *National Centers for Environmental Prediction* (NCEP; Kalnay et al. 1996). The data used has a 6-hr resolution and extends from January 1948 to February 2012. The spectral spatial resolution is T62 (approximately 2.5°x2.5°) and extends from the surface up to 3 hPa (28 vertical levels). Additionally, data from the *European Centre for Medium-Range Weather Forecasts* (ECMWF) ERA-40 (Uppala et al. 2005) is considered. The data starts in September 1957, ends in March 2002, and is available 6-hourly with a spectral spatial resolution of T159 (~1.125°x1.125°). The 60 vertical levels reach 0.1 hPa.

The sea surface temperature (SST) and sea ice data from the *Met Office Hadley Centre* (HadISST) are used. This monthly global dataset starts in 1870 and has a 1°x1° resolution (Rayner et al. 2003). The ocean heat content is estimated from the integrated temperature from 0 to 300 m from the Simple Ocean Data Assimilation (SODA) reanalysis (Carton and Giese 2008). The monthly fields have a horizontal resolution of 0.5˚x0.5˚ and span 1950-2009.

We consider a coupled 505-yr control simulation with pre-industrial external forcing conditions (from year 1860) performed with the ECHAM5/MPIOM1 GCM (hereafter ECHAM5; Roeckner et al. 2003; Jungclaus et al. 2006). The atmospheric (oceanic) model has a spatial resolution of T63 (T31), with 31 (40) vertical levels from the surface up (down) to 10 hPa (5720 m). Oceanic and atmospheric models are coupled without further flux adjustments. The tropical SST variability is found realistic (Jungclaus et al. 2006). The storm track and NAO variability have also been evaluated in previous studies (e.g., Bengtsson et al. 2006; Pinto et al. 2011).

3. Methods

Climate indices

Climate indices are based on winter seasonal averages (DJF) using anomalies from the long term mean. When not mentioned explicitly, a 31-point Lanczos filter with 11-yr. cut-off frequency is applied to the ECHAM5 data to separate interannual and multi-decadal timescales of variability. Filtering is not applied to reanalysis data due to the constraints posed by the short time series. Still, most of the spectral power density is concentrated within the band of 1 to 11-yr (cf. Section 4). The following indices are considered:

- The NAO index (Figs. S1a-c), defined as the leading EOF of 500-hPa geopotential height (z500) winter seasonal anomalies over the area (20-80˚N, 80˚W-40˚E; Barnston and Livezey 1987).
- The Arctic Oscillation (AO, Figs. S1d-f) and Pacific North American Pattern (PNA, Figs. S1g-i), defined as the two leading EOFs of z500 winter hemispheric anomalies north of 20ºN (NOAA CPC definition).
- The Niño-34 index (Figs. S2a-c), based on winter averaged high-pass filtered (1-13 yr.) SST anomalies over the area (5ºS-5ºN, 170º-120ºW; Trenberth 1997).
- The Atlantic Multi-decadal Oscillation (AMO, Figs. S2d-e) index, defined as the leading EOF of SST winter seasonal low-pass filtered anomalies (>13-yr; detrended) over the area (0-70˚N, 95˚W-30˚E; Mohino et al. 2011). For the GCM, the AMO index is calculated as the winter seasonal low-pass filtered SST anomalies over the same area (Fig. S2f; Knight et al. 2005), due to the difficulty of the model in reproducing a realistic EOF1 pattern.
- The Interdecadal Pacific Oscillation (IPO, Figs. S2g-i) index, defined as the leading EOF of SST winter seasonal low-pass filtered anomalies (>13-yr; detrended) over the area (45˚S-80˚N, 120˚E-95˚W; Villamayor and Mohino 2015).
- The Atlantic Meridional Overturning Circulation (AMOC, Fig. S2j) index, defined as the maximum streamfunction of the zonally integrated meridional overturning in the Atlantic Ocean (30˚S-60˚N, 85˚W-20˚E; 500 - 5700 m depth). A low pass filter is applied to the meridional velocity data (>13-yr) to retain the long term variability. Velocity data above 500 m depth are disregarded to avoid wind driven effects on the circulation (Zhang and Wang 2013).

All indices are normalized - divided by their standard deviation. Additionally, the upper-level (500-300 hPa) and lower-level (850-700 hPa) maximum Eady Growth Rate (*bi*; Hoskins and Valdes 1990) is used as indicator of the large-scale baroclinicity and potential wave growth (1):

$$bi = 0.31 \left(\frac{f}{N}\right) \left|\frac{\mathrm{dv}}{\mathrm{dz}}\right|, \quad (1)$$

where f is the Coriolis parameter, N the static stability, z the vertical coordinate and v the horizontal wind vector.

Cyclone Statistics

A cyclone identification and tracking scheme (Murray and Simmonds 1991), adapted and validated for the Northern Hemisphere storm track (Pinto et al. 2005), is applied to 6-hourly winter (DJF) MSLP data. Cyclones are identified using the Laplacian of MSLP, an indicator of their geostrophic relative vorticity. Derived cyclone statistics compare well with other tracking schemes (Raible et al. 2008). Systems are selected based on the following criteria (Pinto et al. 2009): (i) cyclone lifetime ≥ 24 h; (ii) minimum MSLP (p) < 1000 hPa; (iii) Max. (∇^2p) > 0.6 hPa deg.lat.$^{-2}$; and (iv) Max. d/dt ∇^2p ≥ 0.3 hPa deg.lat.$^{-2}$ day^{-1}. The maximum normalized deepening rate (*NDR*) is used as a measure of cyclone's intensity (2):

$$NDR = \frac{\Delta P}{24}\frac{\sin 60^\circ}{\sin \emptyset}, \quad (2)$$

where ΔP is the pressure fall (hPa) and Φ the mean latitude of the cyclone's surface centre over a period of 24 hours. Depending on their maximum *NDR*, cyclones are separated into two 2 different subsets: (i) explosive cyclones (EC; *NDR* ≥ 1 Bergeron); and (ii) non explosive cyclones (NoEC; *NDR* < 1 Bergeron). Cyclone track-densities are constructed by counting the number of cyclones intercepting a circle of radius 7.5 deg.lat. for each grid point over time, providing combined information of cyclone numbers and track lengths.

Statistics Tests

Different methods are applied for statistical hypothesis testing (von Storch and Zwiers 1999): (i) a two tailed t test that accounts for autocorrelation of the series (Bretherton et al. 1999); (ii) a t test for a difference in mean; (iii) a Mann-Whitney U test; and (iv) a Fisher's test for a difference in variance. The confidence intervals chosen are 95% or 99%.

4. Explosive cyclone variability in the reanalysis data sets

A) Interannual variability of explosive cyclone tracks

In this section an analysis of explosive cyclone variability is presented for both reanalysis datasets. We focus on NCEP reanalysis because it spans a longer time period, but ERA-40 results are also discussed where appropriate. The mean track densities of explosive (EC) and non-explosive (NoEC) cyclones are shown in Fig.

1a (NCEP 1948-2011). For EC, a maximum extending from Newfoundland to Iceland is identified. This maximum is consistent with cyclogenesis over the region of strongest baroclinicity near the Gulf Stream (Sanders and Gyakum 1980; Hoskins and Valdes 1990) and subsequent intensification of the storms as they cross the jet (Uccellini 1990; Gilet et al. 2009; Rivière et al. 2013). For NoEC, the area of maximum density is shifted northeastward, extending between southeast Greenland, northwest of the British Isles and Scandinavia.

In order to characterize the variability of winter cyclone activity, the leading Empirical Orthogonal Function (EOF) of cyclone track density anomalies is determined for the entire North Atlantic [20º-80ºN; 90ºW-40ºE] using NCEP reanalysis (Fig. 1b). This analysis includes all cyclones, i.e., explosive and non-explosive systems. The EOF pattern is hereafter labeled with the subscript $_T$ (total). The leading pattern ($All1_T$) represents a latitudinal shift of cyclone trajectories between Iceland and Western Europe. The leading EOF of 250-hPa zonal wind anomalies ($Jet1_T$) and the climatological jet are also overlaid in Fig. 1b. The $Jet1_T$ pattern is consistent with the NAO variability, i.e., with a northward (southward) latitudinal displacement and intensification (weakening) of the extra-tropical jet during the positive (negative) phase. The spatial correspondence between $All1_T$ and $Jet1_T$ latitudinal nodes is evident in Fig. 1b, and is consistent with the steering of cyclone trajectories by the NAO (e.g., Hurrell et al. 2003; Pinto and Raible 2012). The stronger track density center of action over Iceland (Fig. 1b) suggests increased cyclone activity over the sub-polar region in agreement with a positive NAO phase (Pinto et al. 2009).

The leading EOF of explosive cyclone tracks ($EC1_T$) is compared to $Jet1_T$ and the jet core in Fig. 1c. The $EC1_T$ pattern looks also related to the $Jet1_T$ anomalies, but in this case the jet and NAO variability appear to intensify/weaken explosive cyclone activity along their climatological trajectories rather than change the cyclone pathways. This pattern is consistent with the NAO-induced changes in North Atlantic baroclinicity, which is stronger and broader under the NAO positive phase (Pinto et al. 2009). In addition, EC forming over Eastern North America typically cross the upper-level jet from the right-entrance to the left-exit regions, and explosively amplify (Uccellini 1990; Rivière et al. 2013). In contrast, a weaker, less extended and southerly displaced jet is obviously less efficient for explosive intensification.

For completeness, the second leading EOFs of all cyclones ($All2_T$) and explosive cyclones ($EC2_T$) are provided as supplementary material in Figs. S3a-b. $All2_T$ represents a north to south dipole of cyclone trajectories between northern Europe and the Mediterranean (Fig. S3a). $EC2_T$ reveals a different pattern, with an intensification/extension of the explosive tracks between the east coast of the US and the British Isles, and a weakening northeast of Iceland (Fig. S3b). $EC2_T$ is consistent with $Jet2_T$ (250-hpa zonal wind EOF2), a large-

224 scale configuration known to foster the occurrence of explosive cyclogenesis and storm families over Western
225 and Central Europe (Fig. S3b; Hanley and Caballero 2012; Pinto et al. 2014).

226 All1$_T$/EC1$_T$ are significantly (95% confidence interval) correlated with Jet1$_T$ (0.92/0.72), the NAO
227 (0.91/0.78) and the AO (0.78/0.63) for NCEP (Table 1). Likewise, All2$_T$ and EC2$_T$ also significantly correlate
228 with Jet2$_T$. Most of the spectral power for these modes is concentrated within the range of periods 1-11 yr. (Fig.
229 S3c for EC1, not shown for the others). All the modes are well separated (Fig. S2d; North et al. 1982).

230 For comparison, the mean track density pattern and corresponding EOF modes of ALL1$_T$/ALL2$_T$,
231 EC1$_T$/EC2$_T$, and Jet1$_T$/Jet2$_T$ are also calculated for 1957-2001 using ERA-40 (Fig. S4). The ERA-40 track
232 density pattern (Fig. S4a) is very similar to NCEP, but with a greater total number of cyclone counts. This may
233 be due to the higher horizontal resolution of ERA-40 (Pinto et al. 2005). The EOFs are also similar to NCEP
234 (Fig. S4b-e) and represent the same variability (Table 1). The modes are well separated (Fig. S3d). In general
235 terms, the linear correlation results between EC1$_T$ and Jet1$_T$ agree well in both reanalysis (Table 1), with slightly
236 lower values for NCEP (ERA-40: 0.85; NCEP: 0.72). However, if the same time period is considered, the values
237 are almost identical (NCEP: 0.83). Thus, in the next section this apparent time-evolving correlation is analyzed
238 in more detail.

239

240 **B) Analysis of stationarity**

241 In order to assess the stationarity of the relation between the NAO and explosive cyclogenesis, 21-year
242 running correlations between the leading Principal Components (PCs) of EC1$_T$ and NAO$_T$/Jet1$_T$ are shown in
243 Fig. 1d for NCEP and ERA-40. The analysis suggests a non-stationary link between the NAO$_T$/Jet1$_T$ variability
244 and EC1$_T$ in NCEP. Specifically, the NAO$_T$/Jet1$_T$ influence on EC1$_T$ is particularly weak at the beginning of the
245 period, increases abruptly in the 60s and remains large to the late 90s (solid blue/red curves in Fig. 1d). In ERA-
246 40 (Fig. 1d; dashed blue/red curves), the time series are too short to detect any change in the correlation.
247 Nevertheless, the ERA-40 results are consistent with NCEP between the 60s and 90s.

248 In order to analyze possible dynamical differences between the two NCEP periods, EOFs are calculated
249 independently for winters 1948-1962 (labeled as 50s; e.g. EC1$_{50s}$/Jet1$_{50s}$) and 1963-1997 (labeled as 80s). All
250 EOFs are standardized with respect to the PC for the full period. Figs. 2a-b show that the leading mode of
251 explosive cyclone track density is sensitive to the choice of period. The 1948-1962 EOF1 for explosive cyclones
252 (EC1$_{50s}$; Fig. 2a) is constrained over the western North Atlantic, showing a strengthening/weakening of the
253 cyclone tracks between Eastern North America and southern Greenland. The structure of the associated Jet1$_{50s}$

depicts a latitudinal jet variability also constrained to the westernmost part of the basin (Fig. 2a). In contrast, the spatial structure of $EC1_{80s}$ is similar to $EC1_T$ (Fig. 2b) and explains more variability (40 vs. 36%). The $EC1_{80s}$ pattern is centered over the northeastern North Atlantic, with a maximum over Iceland.

For the jet variability ($Jet1_{80s}$; Fig. 2b), both latitudinal centers of action are stronger than for $Jet1_{50s}$ (Fig. 2a) and span the entire North Atlantic basin, explaining a much larger fraction of variance (56 vs. 32%). The z500 anomalies of each period are regressed on the corresponding EC PCs (Figs. 2c-d, respectively). A pattern consisting of three centers of action over the North Atlantic is found for the first period (1948-1962), with positive anomalies over the western sub-tropical North Atlantic and Western Europe, and a negative anomaly south-west of Greenland. In contrast, the second period (1963-1997) features a very clear NAO/AO hemispheric structure, with significant seesaw anomalies spanning over the whole North Atlantic.

Differences in the NAO patterns calculated independently for each period (NAO_{50s} vs. NAO_{80s}, Figs. 2e-f) are consistent with differences in the regressed z500 patterns (Moore et al. 2013). In particular, the sub-tropical NAO center of action appears weaker over the central North Atlantic in the first period, and two separated maxima are found over Eastern North America and Europe (Fig. 2e). The positive maximum over Europe may hinder the extension of cyclone tracks over the eastern North Atlantic in $EC1_{50s}$ (Fig. 2a). The spatial correlation between NAO_{50s} and NAO_T is only 0.50. These results are consistent with Raible et al. (2014), who provided evidence based on the 20CR reanalysis that the z500 teleconnectivity between Baffin Island and the western North Atlantic is dominant for the period 1940-1969 (cf. their Fig. 5b). For the second period, a very strong, extensive, zonally symmetric and eastward displaced NAO is observed (Fig. 2f), which is consistent with enhanced cyclone activity over the eastern sub-polar North Atlantic (Fig. 2b). This NAO_{80s} pattern shows a much higher spatial correlation with the total period NAO_T (0.86).

The winter SST anomalies of each period are also regressed on the EC PCs (Figs. 2g-h). A significant cooling over the sub-tropical and sub-polar North Atlantic is associated with the positive phase of $EC1_{80s}$ (Fig. 2h), and with warming in the central part of the basin. This Atlantic SST tripole pattern is typical of the positive phase of the NAO, whose subtropical part is found to have predictive skill (Czaja and Frankignoul 1999; Rodríguez-Fonseca et al. 2006; Losada et al. 2007). The regressed SST pattern has the same sign over the winter equatorial Pacific and sub-tropical north Atlantic, as is well described in the literature (Fig. 2h; Wang 2002; Sung et al. 2013). During the 50's period, a stronger connection with the North Pacific SSTs is evident (Fig. 2g), which is consistent with previous analyses (Raible et al. 2001; 2004). Although based on few SST observations,

283 it is striking that the positive relationship between the equatorial Pacific and the sub-tropical North Atlantic
284 anomalies disappears during the 50's period (Fig. 2g), coinciding with the decoupling between NAO and $EC1_{50s}$.
285
286 **C) Impact of multi-decadal variability**
287 The possible influence of the lower-frequency multi-decadal variability on the connection between explosive
288 cyclogenesis and the NAO is investigated based on the inter-decadal evolution of the jet and maximum Eady
289 Growth Rate. The latter is an indicator of baroclinicity and potential cyclone growth (Hoskins and Valdes 1990).
290 The climatological values of the jet intensity (u250) and Maximum Eady Growth Rate in the upper (500-300
291 hPa; bi400) and lower (850-700 hPa; bi775) troposphere are presented in Figs. 3a and S5a (NCEP). Both bi400
292 and bi775 overlap well with u250 (particularly bi400). The three variables are thus good estimators of the
293 vertical environmental wind shear and potential growth of cyclones (e.g., Pinto et al. 2009). Differences
294 between the two periods (1948-1962 vs. 1963-1997) are shown in Fig. 3b. The early period is characterized by a
295 weaker jet and decreased baroclinicity (bi400) over large parts of the sub-polar North Atlantic compared with
296 the second period, with more suitable conditions for cyclone formation over the sub-tropical North Atlantic. For
297 the lower level baroclinicity (bi775; Fig. S5b), large differences are observed over western Greenland. The
298 strong low level baroclinicity over Western Greenland during the first period might explain the deflected EC
299 trajectories toward this region in the $EC1_{50s}$ pattern (cf. Fig. 2a). In addition, no significant change in bi775 is
300 observed over the sub-tropical North Atlantic between the two periods, in contrast with the bi400 results (cf.
301 Figs. 3b and S5b). The bi400 changes might be related to the modified intensity of the sub-tropical jet, which is
302 confined to the upper troposphere.
303 To analyze the decadal jet and NAO variability for the NCEP period, a Hovmöller diagram of low-pass
304 filtered (>33 yr.) u250 anomalies averaged between 100°W-20°W, an index of the latitudinal location of the
305 maximum positive jet anomalies and a multi-decadal NAO index are presented in Fig. 3c. The latter is shifted
306 and rescaled to have the same mean and standard deviation as the latitude index. The period of low correlation
307 between $EC1_T$ and $Jet1_T/NAO_T$ (1948-1962) is characterized by minimum values in the jet latitude index and in
308 the decadal NAO, and by negative u250 anomalies spanning over the latitude band 40˚-60˚N (Fig. 3c). In
309 contrast, a more intense and poleward shifted jet is observed during the latter period, together with a more
310 positive decadal NAO.
311 The influence of inter-decadal changes in the ocean is analyzed through the winter SSTs and integrated (0-
312 300 m) ocean temperature. Climatologies of these variables are shown in Fig. S5c. Fig. 3d shows the winter SST

difference between the two periods: a positive anomaly pattern apparently reminiscent of the Atlantic Multi-decadal Oscillation (AMO; Knight et al. 2005) is found over the North Atlantic. This is consistent with the observed out-of-phase relation between the EC-NAO/Jet running-correlations and the AMO index (Fig. 1d). Thus, the strengthening and eastward propagation of EC track density during the second period (Fig. 2b) could be associated with a more negative AMO phase. Both changes could be driven by the AMOC (Sun et al. 2015), greenhouse gas forcing, or both (Woollings et al. 2012).

The difference in winter integrated temperature (0-300 m, T300) is shown in Fig. S5d as an indicator of changes in the ocean heat content above the thermocline. The emerging pattern seems consistent with the impacts of AMO and AMOC, with significant cooling in the tropics (Wang and Zhang 2013, cf. their Fig. 1). The inter-decadal changes between the 50s and 80s in terms of the meridional T300 gradient (δyT300) are also depicted in Fig. S5d. Significant changes in δyT300 are found over the tropical North Atlantic, but not over extratropical areas.

We hypothesize that decadal variations of the jet and the ocean may contribute to modulate inter-decadal changes in the interannual variability of explosive North Atlantic cyclones. However, the robustness of these results is difficult to establish given the short time series. In particular, it is not clear if the variability changes in EC activity are triggered by natural decadal variability of the climate system, anthropogenic climate change (e.g., the eastern NAO shift during the late 20th century, a slowdown of the AMOC, etc.) or are just fortuitous. These facts put forward the necessity of using long control simulations in order to better infer a robust hypothesis about the mechanisms involved and characterize EC variability at longer timescales.

5. Explosive cyclone variability in ECHAM5/MPIOM1

A) Multi-decadal variability of explosive cyclone tracks

We next describe the variability of explosive cyclones in a 505-yr long control simulation with the ECHAM5/MPIOM1 coupled model. First, a broad overview of the multi-decadal cyclone variability is provided, which could not be analyzed with the shorter reanalysis data sets.

Cyclone track density GCM climatologies for EC and NoEC are shown in Fig. 4a. Just like NCEP (Fig. 1a), the maximum in EC activity is located between Newfoundland and Iceland. For NoEC, the shape and counts are also similar to NCEP over the North Atlantic. The main difference between ECHAM5 and NCEP for EC densities (Fig. 4b) is that ECHAM5 produces too zonal tracks - a systematic bias in GCMs (e.g., Zappa et al. 2014; Seiler and Zwiers 2015). The same is found for NoEC (not shown).

343 The leading EOFs of low-pass filtered (>11-yr) EC track density data are calculated. The leading modes of
344 variability at multi-decadal timescales are very similar to the unfiltered modes found for reanalysis (cf. section
345 4). In particular, $EC1_{LF}$ (Fig. 4c; LF stands for low frequency) also represents a strengthening/weakening of EC
346 tracks between Newfoundland and Iceland. $EC2_{LF}$ (Fig. S6a) depicts a similar pattern southerly shifted between
347 eastern North America and Western Europe. The leading EOFs of low pass filtered (>11-yr) u250 winter
348 anomalies reveal again very similar structures to the interannual modes. Please note the different scales used in
349 Figs. 4 and S6 due to the different amplitude of this variability.
350 Linear correlations between the PCs of these modes and dominant low-frequency teleconnection patterns
351 (e.g., decadal NAO, AMO, IPO etc.) are provided in Table 2. Correlations show that $EC1_{LF}$ is tightly connected
352 with decadal variability of the NAO (NAO_{LF}; 0.75) and the jet ($Jet1_{LF}$; 0.68). $EC2_{LF}$ is significantly anti-
353 correlated (correlated) with $Jet1_{LF}$ ($Jet2_{LF}$). These results suggest that multi-decadal fluctuations of EC tracks
354 and frequencies are primarily controlled by the decadal variability of the NAO and the jet.
355
356 **B) Interannual variability of explosive cyclone tracks**
357 In order to test the robustness of the results from section 4, the interannual (1-11 yr.) variability of EC
358 density tracks is also analyzed in ECHAM5/MPIOM1. The leading interannual EOF of explosive cyclones for
359 the whole period ($EC1_T$) represents a strengthening/weakening of the climatological pattern between
360 Newfoundland and Iceland (Fig. 4d), also consistent with EOF1 of u250 ($Jet1_T$).
361 The winter anomalies of z500 for the total ECHAM5 period are regressed on the $EC1_T$-PC (Fig. 4e),
362 revealing again a very clear AO/NAO pattern (cf. Table 1). This pattern is very similar to that obtained for the
363 second NCEP period (Fig. 2d). The winter SST anomalies are also regressed on $EC1_T$-PC (Fig. 4f), resulting in a
364 pattern very similar to the second NCEP period (Fig. 2h). In particular, both the North Atlantic tripole pattern
365 and ENSO appear to be significantly correlated and anti-correlated, respectively, with the leading mode of
366 variability of explosive cyclone tracks. These results contrast with the non-significant ENSO-EC1 connection
367 found in NCEP (Fig. 2h). However, as already mentioned, results from observations should be considered with
368 caution due to the short time series of available data.
369 Finally, the remaining EOFs ($All1_T$, $All2_T$, $EC2_T$) are provided in Figs. S6b-d. These are again in good
370 agreement with NCEP and ERA-40.
371
372 **C) Analysis of stationarity**

To investigate whether the non-stationary behavior found in NCEP is also present in the GCM and to what extent these results are caused by natural variability of the climate system, the time-dependent relation between $EC1_T$ and the $Jet1_T/NAO_T$ variability is analyzed. We focus on the interannual (1-11 yr.) variability, as the spectral density of the reanalysis is mainly concentrated within the band 1-11 yr (cf. Fig. S3c). Fig. 5a shows the 21-yr running correlations between the principal components (PCs) of $EC1_T$ and the $NAO_T/Jet1_T$. $EC1_T$ and NAO_T are highly correlated most of the time, but appear to be less correlated or 'decoupled' in specific periods. The same is found for $EC1_T$ vs. $Jet1_T$ PCs. Hereupon we refer to the periods of low correlation as 'decoupling periods' (51 years in total, model years 182-209 and 305-327; Fig. 5a). Although smoothed, the 'decoupling periods' can still be detected in the running correlations if the window length is increased to 41-yr.

We analyze the change of the leading patterns of variability during the simulation with running EOFs. If the EC or NAO variability changes during specific periods, the EOFs for those periods are expected to look differently. With this aim, we compute the EOFs in 21-yr sliding windows (485 patterns for 505 years) with a consistent polarity for all calculations.

On the one hand, the spatial correlation between each of the 485 NAO patterns and the total period NAO_T is shown in Fig. 5b. There are no abrupt changes in the correlations during the decoupling periods, suggesting that the NAO spatial structure could remain largely unchanged. However, visual inspection of the spatial NAO pattern calculated only for the decoupling dates (Fig. 5c; hereafter NAO_D) reveals a noticeable strengthening of its southern node compared with NAO_T (Fig. S1c). This is suggestive that the NAO spatial correlation values in Fig. 5b could be more sensitive to the location of the NAO centers of action than to their relative strength. As will be described later on, the relative intensity of the NAO nodes and their projection onto the mean flow seems to be determinant for explosive cyclone development over the North Atlantic.

On the other hand, the spatial correlation between the time-varying and total-period explosive cyclone modes is non-stationary in time and changes abruptly during the decoupling periods (Fig. 5b). This suggests that the occurrence of the decoupling periods is due to a clearly different spatial structure of the leading EC variability. A zonal average (90˚W-40˚E) of each of the 485 EC1 regression patterns is performed to characterize these changes. An index with the latitudinal location of the maximum positive center of action for each EC1 pattern is displayed in Fig. 5b, and shows an abrupt southward shift of this center of action (from ~60˚N to 45˚N) during the decoupling periods. This is confirmed when the specific EOF1 of explosive cyclone track density anomalies is calculated solely for the decoupling dates ($EC1_D$; Fig. 5d). Here, $EC1_D$ represents a strengthening/weakening of the explosive cyclone tracks between Eastern North America and Western Europe, a

403 pattern shifted south relative to the total period $EC1_T$ (compare Figs. 4d and 5d). Finally, the corresponding
404 second leading EOF ($EC2_D$) depicts an intensifying/weakening pattern more constrained over the Icelandic area
405 (Fig. S6e). This suggests that the two leading EOFs change order during the decoupling periods.

406 Although the leading variability of EC track density is normally explained by a pattern confined over the
407 northern sub-polar regions, the variability shifts south during specific periods and cannot be explained by the
408 EOFs computed for the full period ($EC1_T$ and NAO_T). Unlike NCEP, these changes do not appear to be
409 associated with a pure longitudinal shift of the NAO nodes, but with modifications in their relative strength. The
410 potential changes in the interannual forcing during the decoupling periods are investigated through the
411 regression of z500 and SST winter anomalies on $EC1_D$-PC (Figs. 5e-f). During these periods, the z500 pattern
412 associated with the variability of EC is characterized by a belt of low pressure anomalies extending from
413 Newfoundland to Western Europe between 40°-60°N (Fig. 5e). This anomaly is accompanied by positive
414 anomalies of z500 between Greenland and Scandinavia and over the eastern sub-tropical North Atlantic
415 (~30˚N). The sign and shape of the z500 anomalies do resemble the NAO- pattern. Indeed, the correlation
416 between $EC1_D$ and $Jet1_D$/NAO_D is -0.62/-0.49 (99% confidence interval). Therefore, explosive cyclones appear
417 to be favored by NAO- during the decoupling periods, in contrast with the normal situation. It will be shown in
418 section 5E that the baroclinicity associated with the negative NAO years during the decoupling periods is
419 stronger and more extensive over the North Atlantic than that for the positive NAO years (unlike the
420 climatology; cf. Pinto et al. 2009). Regarding the SST anomalies, no significant regression pattern is found (Fig.
421 5f), nor there is an indication of the North Atlantic SST tripole during the decoupling periods.
422
423 **D) Impact of multi-decadal variability**
424 The potential role of multi-decadal variability as modulator of interannual EC variability is analyzed in the
425 following. During the decoupling periods, EC is anomalously frequent in the corridor between the eastern US
426 and Western Europe, while their numbers are reduced from southern Greenland to Western Scandinavia (Fig.
427 6a). A similar structure is observed in the variance, with an increase of variability to the south and a decrease to
428 the north. This is consistent with greater variability in the areas where EC are more frequent. In contrast, no
429 significant differences are observed in the mean or in the variance of the North Pacific storm track (not shown).
430 This suggests that the westerly flow from the North Pacific does not play an important role in the occurrence of
431 the decoupling periods.

This raises again the question of why EC tracks shift south during long and persistent periods of time (~20-25 years each). The long term anomalies of the jet intensity and the upper-level maximum Eady Growth Rate are calculated for the decoupling periods. The climatological means for ECHAM5 are provided in Fig. 6b for comparison. The overlapping between both variables is evident, although with a much more zonal structure than for NCEP. During the decoupling periods both the jet and bi400 significantly shift south (Fig. 6c), with positive anomalies over the sub-tropical North Atlantic and negative values over the Newfoundland-Iceland area. The same is observed for bi775 (not shown). Thus, the long-term upper-level conditions become more efficient for cyclone growth between the eastern US and Western Europe at the expense of the sub-polar North Atlantic.

The low-pass filtered (>33-yr) u250 anomalies averaged between 100˚-20˚W are used to highlight the latitude of the maximum positive jet anomalies in Fig. 6d. The decadal NAO index is also shown. The polar jet exhibits strong multi-decadal variability, with multiple oscillations in the latitude range 30˚-65˚N.

It is noticeable that both decoupling periods feature a persistent and remarkably equatorward shifted jet. Moreover, weakened upper-level winds are identified around 45˚-60˚N (consistent with Fig. 6c). Although the low-frequency variability of the NAO and the jet appear similar in Fig. 6d, it is noteworthy that the decadal NAO index has lower amplitude during the decoupling periods. Therefore, additional potential forcings for the southward shift of the jet are investigated.

Eddy-driven jets tend to be located over areas with maximum meridional SST and ocean heat content (OHC; total heat content above the oceanic thermocline) gradients (cf. Figs. 7a and S7a; Minobe et al. 2008; Nakamura et al. 2008). Therefore, we hypothesize that if the North Atlantic SST/OHC meridional gradient shifts in latitude during specific periods, then the extra-tropical jet and baroclinicity fields might also respond to this forcing (Dong et al. 2013). This is observed for the SST and OHC anomaly during the decoupling periods (Fig. 7b). During these periods, an extensive cold SST anomaly is present across the sub-tropical North Atlantic. Such anomaly extends over the full mixed layer depth (Fig. 7b) and below the thermocline (Fig. S7b). As a consequence, a significant attenuation of the meridional OHC gradient is observed over the Gulf Stream area during the decoupling periods, together with an increase over the sub-tropical North Atlantic (Fig. 7c). Such a SST/OHC anomaly pattern is thought to: (i) force positive jet and baroclinicity anomalies over the sub-tropical North Atlantic; and (ii) support the persistence of these anomalies through a positive feedback process. A southerly shifted storm track cools the waters beneath, which acts to reinforce the pre-existing SST anomaly (Dong et al. 2013). As a note of caution, it must be noted that these gradient anomalies (Fig. 7c) are particularly weaker than in Nakamura et al. (2008). To evaluate the potential forcing of these oceanic anomalies, several

462 indices of temperature anomaly in the mixed layer are constructed for the North Atlantic area (30˚-40˚N, 60˚-
463 30˚W; dashed rectangle in Fig. 7b). Fig. 7d shows the low pass filtered (>33-yr) indices of ocean temperature
464 anomaly in depth. As expected, they reveal exceptional negative anomalies over the focus area during the
465 decoupling periods. The AMOC index calculated for the MPIOM1 data is also provided in Fig. 7d (cf. AMOC
466 pattern in Fig. S2j) and significantly correlates with the indices of ocean temperature anomaly: AMOC vs. SST
467 = 0.35; AMOC vs. T123m = 0.60 (99% confidence interval). However, the overlapping is not so evident for all
468 the periods (e.g., second decoupling period). We speculate that the AMOC could play a role for the occurrence
469 of the decoupling periods in agreement with an equatorward shift of the extra-tropical jet and baroclinicity, but
470 the degree of this influence is uncertain. In this line, a deficient representation of the AMOC strength in climate
471 models appears to lead to important SST biases over the North Atlantic (Wang et al. 2014). Despite the obtained
472 AMOC pattern in ECHAM5/MPIOM1 looks strong enough (cf. Fig. S2j), the model bias could exert as well
473 some undesired influence in the dynamics observed during the decoupling periods.
474 In the next section, we discuss possible atmospheric mechanisms explaining the changes in the NAO-EC
475 relation during the decoupling periods based on these ingredients.
476
477 **E) Potential mechanisms leading to the Decoupling Periods**
478 In this section, we propose two different mechanisms to explain the abrupt transitions in the EC leading
479 variability and its connection with the NAO.
480 • The *cross-jet* mechanism: Under normal conditions, the interannual jet alternates its position
481 between the northern, central and southern North Atlantic locations during consecutive years
482 (Fig. 8a; Woollings et al. 2010). When the jet is situated over its northern position (NAO+), low
483 pressure systems forming over eastern North America can easily cross the extra-tropical jet and
484 explosively amplify (Fig. 8a; cf. Uccellini 1990; Gilet et al. 2009; Rivière et al. 2013). Under a
485 negative NAO phase, the relative position between developing cyclones and the jet is less efficient
486 for rapid cyclone intensification, and explosive cyclone deepening is thus weaker over the North
487 Atlantic. This mechanism is consistent with the NAO modulation of explosive cyclone variability
488 identified for most of the time periods in the GCM. However, when the interannual jet is
489 persistently (20-25 yr.) located over the central or sub-tropical North Atlantic (i.e. a southerly
490 shifted multi-decadal jet), the EC variance associated with NAO+ years is absent. This implies that
491 NAO+ no longer acts as a precursor for explosive cyclone deepening; instead, a different mode of

EC variability emerges (Fig. 8b). For this mechanism to occur the jet locations must significantly vary with the NAO phase but the main genesis area of explosive cyclones over Eastern North America must not, which is the case in our results (cf. Figs. 8ab). Thus, we consider the *cross-jet* mechanism as a plausible hypothesis for the occurrence of abrupt transitions in the EC variability and the decoupling periods.

- The *NAO-barolinicity* mechanism: Under normal conditions, the North Atlantic baroclinicity associated with NAO+ is stronger and extends over a broader region than for NAO- (Pinto et al. 2009). Consistent with this, the number of explosive cyclones over the North Atlantic is higher (lower) under NAO+ (NAO-). However, the opposite is found during the decoupling periods, when explosive cyclones seem to be favored under NAO-. To check if this might be due to changes in NAO-mediated baroclinicity, composite maps of total upper-level baroclinicity (bi400) are computed for NAO values above and below ±1 SU for climatology (NAO_T) and decoupling periods (NAO_D). These maps are shown in Figs. 9a-d, with the areas of highest bi400 (>40 day^{-1}) emphasized with stippling. The baroclinicity associated with NAO+ appears to be more intense/extensive than for NAO- in climatology (Figs. 9ab). For the decoupling periods the contrary is observed (Figs. 9cd). For a more quantitative comparison, the total sum of actual values over grid points with highest bi400 (stippled areas; disregarding the subtropical jet) is determined to estimate the baroclinicity strength/extent under each situation. In Fig. 10, the total values for each case (in %, normalized with the climatology/NAO+ case) are provided. As expected, results depict a higher (lower) baroclinicity under NAO- (NAO+) during the decoupling periods (as opposed to climatology). The same is observed if a more relaxed criterion of 35 day^{-1} is used (not shown).

Both the *cross-jet* and *NAO-baroclinity* mechanisms are plausible hypotheses which could contribute to the abrupt transitions in EC variability in ECHAM5/MPIOM1 during the decoupling periods, and it is not obvious which of the two is more relevant. To answer this question, regional simulations forced to different large-scale configurations would be useful. Such an approach is outside the scope of the paper and is left for future work.

6. Summary and conclusions

This study explores the modulating role of the multi-decadal oceanic and atmospheric variability (>11-yr) on the interannual climate variability (1-11 yr.) of explosive cyclogenesis over the North Atlantic in wintertime. In addition, the multi-decadal variability of explosive cyclone tracks is assessed. For this purpose, the track density

522 of explosive and non-explosive cyclones from two reanalysis datasets and a long control General Circulation
523 Model (GCM) simulation are analyzed. An Empirical Orthogonal Function (EOF) approach is used to
524 characterize the preferred modes of variability in the North Atlantic.

525 Results show that the leading mode of the interannual climate variability for all cyclones ($All1_T$) represents
526 primarily a latitudinal shift of cyclone trajectories between Iceland and Western Europe (Fig. 1b). This pattern is
527 consistent with previous studies (e.g., Rogers 1997; Lu and Greatbach 2002). However, the leading interannual
528 variability mode of explosive cyclone tracks ($EC1_T$) consists of a strengthening/weakening of its climatological
529 pattern extending from Newfoundland to Iceland (Fig. 1c). Although these two patterns are different, both
530 modes are significantly correlated with the North Atlantic Oscillation (NAO) during most time periods in all
531 three datasets (cf. Table 1). This results from the influence of the NAO in modulating cyclone's trajectories
532 ($All1_T$; cf. Wanner et al. 2001) and cyclone intensification rates ($EC1_T$; cf. Pinto et al. 2009). However, during
533 specific decades of NCEP and ECHAM5, the EC1-NAO correlation abruptly drops.

534 For NCEP, this non-stationary relationship is apparently associated with multi-decadal changes in the NAO
535 shape and location. In particular, the NAO-EC1 correlation is 0.68 between 1948 and 1962. In this period the
536 NAO pattern is more confined over the western North Atlantic (Raible et al. 2014). Contrastingly, the period
537 1963-1997 is characterized by an eastward extension and intensification of the NAO centers of action (Jung et
538 al. 2003). During this period, the NAO-EC1 correlation increases to 0.89. The changes in the NAO structure are
539 consistent with the changes in EC1 between periods. Thus, EC1 is more confined west in the basin during the
540 mid 20th century, whereas for recent decades it appears stronger and more extended towards Northern Europe
541 (cf. Fig. 2). These decadal changes in NAO and EC1 variability appear to coincide with changes in the Atlantic
542 Multi-decadal Oscillation phase (AMO; Woollings et al. 2012).

543 For ECHAM5, the NAO-EC1 correlation is constant and positive during most of the simulation, except for
544 two periods about 20-25 yr. long (Fig. 5). During these periods (so called 'decoupling periods'), EC1 abruptly
545 changes shape and the NAO-EC1 correlation rapidly switches to negative values. In this article two different
546 potential mechanisms have been proposed to explain such behavior:

547 - The first is the so called *cross-jet* mechanism and relies on the relative position between the eddy-
548 driven jet (Woollings et al. 2010) and explosive cyclones growing over eastern North America
549 (Hoskins and Hodges, 2002) during consecutive years (20-25 yr.). This mechanism appears to be
550 related to multi-decadal variability of the atmosphere and the ocean. It occurs during periods when
551 the jet is persistently shifted south, the meridional gradient of ocean heat content over the

552 subtropical North Atlantic is enhanced and the Atlantic Meridional Overturning Circulation
553 (AMOC) is weakened (Figs. 6 to 8).

554 • The second is the so called *NAO-baroclinicity* mechanism. This mechanism relies on multi-decadal
555 variability of the atmosphere, in particular on how multi-decadal changes in the NAO structure and
556 relative strength of its centers of action project on interannual variability features. As opposed to
557 climatology (Pinto et al. 2009), the baroclinicity associated with NAO- is stronger and more
558 extensive than for NAO+ over the North Atlantic during the decoupling periods (Figs. 9 and 10). As
559 a consequence, explosive cyclones are favored by NAO- instead of NAO+. These changes lead to
560 abrupt transitions in the EC leading variability mode and the EC1-NAO correlation.

561 The present results evidence the importance of the low-frequency control for the time-evolving interannual
562 climate variability of explosive cyclone tracks in the North Atlantic. This modulation leads to a non-stationary
563 connection between the NAO and EC activity both in reanalysis and GCM data. In this context, a plausible
564 influence of the ocean circulation on this non-stationary connection is highlighted. Although this influence looks
565 different between reanalysis and the GCM, this is not surprising as the low NAO-EC1 correlation periods in
566 both datasets are associated with distinct EOF patterns (compare Figs. 2a and 5d). An interesting question left
567 for future work concerns the relative role played by the ocean in the longitudinal location and relative intensity
568 of the NAO centers of action (Wang et al. 2012; Raible et al. 2014). The opposite effect, in which the NAO
569 triggers multi-decadal changes in the ocean, is also present in the literature (Visbeck et al.1998; Delworth and
570 Greatbatch 2000; Eden and Jung 2001). The NAO positive phase is thought to strengthen the AMOC via air-sea
571 fluxes of heat and momentum (Delworth and Zeng 2015), and induce a basin-wide SST warming (AMO
572 pattern). This pattern subsequently switches phase and behaves as a delayed oscillator, which explains a 60 yr.
573 quasi-periodic cycle of the NAO (Sun et al. 2015). In this work we suggest that AMOC could in turn alter the
574 position of the jet stream and maximum baroclinicity over the North Atlantic, thus modifying the preferred
575 regions explosive cyclone development. The study of the opposite branch of this relation remains as an
576 interesting path for future research.

577 The present results can potentially contribute to an improvement of the multi-decadal predictions of extreme
578 cyclones in the North Atlantic (e.g., Lee et al. 2012; Nissen et al. 2014; Feser et al. 2015). Regarding the
579 potential role of anthropogenic climate change in the NCEP results, it must be noted that abrupt changes in the
580 variability of explosive cyclogenesis are also observed in the pre-industrial simulation, so these transitions can
581 be internally driven.

582 Additionally, an unsteady connection between the EC leading variability and El Niño-Southern Oscillation is
583 also found in the GCM data (Luksch et al. 2005). Such connection must be checked in additional control
584 simulations to potentially improve seasonal predictions of explosive North Atlantic cyclones.

585 At multi-decadal timescales (>11-yr), the main variability mode of explosive cyclones also depicts a
586 strengthening/weakening pattern of EC tracks between Newfoundland and Iceland (Fig. 4c). Our results suggest
587 that this variability is predominantly driven by the decadal NAO and jet variability. Further analysis on this
588 topic is also left for future work.

589 Finally, as this study is mainly focused on explosive cyclogenesis, an extended analysis for all cyclones and
590 their time-varying relation with the NAO will be an interesting path for future research through the use of a
591 larger set of control and forced simulations (e.g., CMIP5 models).

592

593 **Acknowledgements**

594 We thank the *National Centers for Environmental Prediction* and the *European Centre for Medium-Range*
595 *Weather Forecasts* for the NCEP and ERA-40 reanalysis. We thank the *Met Office Hadley Centre* for the SST
596 and sea ice data (HadISST) and the *University of Maryland* for the Simple Ocean Data Assimilation (SODA)
597 reanalysis. We are indebted to the *Max Plank Institute* and the *Deutsches Klimarechenzentrum* (DKRZ) for the
598 ECHAM5/MPIOM1 data. In particular, we thank Hans Winter, Hannes Thiemann, Helmuth Haak and Monika
599 Esch for help with the MPIOM1 data. IG is supported by the research projects MULCLIVAR (CGL-2012-
600 38923-C02-01 - Spanish Ministry of Economy and Competitiveness) and PREFACE (EUFP7/2007–2013 grant
601 agreement 603521). We thank Irene Polo, Marta Martín-Rey, Jorge López-Parages, Rubén Banderas, Tim
602 Woollings and Christoph Raible for constructive remarks. We thank Gwendal Rivière and another anonymous
603 reviewer for their pertinent comments and suggestions, which have contributed to improve this manuscript.

604

605

606 **References**

607 Bader J, Mesquita MDS, Hodges KI, Miles M, Osterhus S, Keenlyside N (2011) A Review on Northern
608 Hemisphere Sea-Ice, Storminess and the North Atlantic Oscillation: Observations and Projected Changes.
609 Atmos Res 101: 809-834. doi:10.1016/j.atmosres.2011.04.007 .

610 Baldwin MP, Dunkerton TJ (2001) Stratospheric Harbingers of Anomalous Weather Regimes. Science 294
611 (5542): 581-584. DOI:10.1126/science.1063315

612 Barnston AG, Livezey RE (1987) Classification, Seasonality and Persistence of Low-Frequency Atmospheric
613 Circulation Patterns. Mon Wea Rev 115: 1083–1126. doi: 10.1175/1520-
614 0493(1987)115<1083:CSAPOL>2.0.CO;2

615 Benedict JJ, Lee S, Feldstein SB (2004) Synoptic view of the North Atlantic Oscillation. J Atmos Sci 61: 121 -
616 144.

617 Bengtsson L, Hodges KI, Roeckner E, Brokopf R (2006) On the natural variability of the pre-industrial
618 European climate. Clim Dyn 27:743–760.

619 Bjerknes J, Solberg H (1922) On the life cycle of cyclones and the polar front theory of atmospheric circulation
620 (edited by Henry AJ). Mon Wea Rev 50: 468–473. doi: http://dx.doi.org/10.1175/1520-
621 0493(1922)50<468:JBAHSO>2.0.CO;2

622 Blackmon ML, Wallace JM, Lau NC, Mullen SL (1977) An Observational Study of the Northern Hemisphere
623 Wintertime Circulation. J Atmos Sci 34: 1040-1053. doi: 10.1175/1520-
624 0469(1977)034<1040:AOSOTN>2.0.CO;2

625 Bosart LF, Lin SC (1984) A diagnostic analysis of the Presidents' Day storm of February 1979. Mon Wea Rev
626 112: 2148 - 2177.

627 Bretherton CS, Widmann M, Dymnikov VP, Wallace JM, Blade I (1999) Effective number of degrees of
628 freedom of a spatial field. J Climate 12: 1990-2009.

629 Carton JA, Giese BS (2008) A Reanalysis of Ocean Climate Using Simple Ocean Data Assimilation (SODA).
630 Mon Wea Rev 136: 2999-3017

631 Chang EKM, Orlanski I (1993) On the Dynamics of a Storm Track. J Atmos Sci 50: 999–1015. doi:
632 10.1175/1520-0469(1993)050<0999:OTDOAS>2.0.CO;2

633 Chen S, Wu R, Chen W (2015) The Changing Relationship between Interannual Variations of the North
634 Atlantic Oscillation and Northern Tropical Atlantic SST. J Climate 28: 485–504. doi: 10.1175/JCLI-D-14-
635 00422.1

636 Czaja A, Frankignoul C (1999) Influence of the North Atlantic SST on the atmospheric circulation. Geophys
637 Res Lett 26 (19): 2969-2972. DOI: 10.1029/1999GL900613
638 Davis CA, Emanuel KA (1988) Observational evidence for the influence of surface heat fluxes on maritime
639 cyclogenesis. Mon Wea Rev 116: 2649 - 2659.
640 Delworth TL, Greatbatch RJ (2000) Multidecadal thermohaline circulation variability driven by atmospheric
641 surface flux forcing. J Clim 13: 1481-1495.
642 Delworth T, Zeng F (2015) The impact of the North Atlantic Oscillation on climate through its influence on the
643 Atlantic Meridional Overturning Circulation. J Clim. doi:10.1175/JCLI-D-15-0396.1
644 Dong B, Sutton RT, Woollings T, Hodges K (2013) Variability of the North Atlantic summer storm track:
645 mechanisms and impacts on European climate. Environ Res Lett 8: 034037. doi:10.1088/1748-
646 9326/8/3/034037
647 Drouard M, Rivière G, Arbogast P (2015) The Link between the North Pacific Climate Variability and the
648 North Atlantic Oscillation via Downstream Propagation of Synoptic Waves. J Climate 28: 3957-3976. doi:
649 10.1175/JCLI-D-14-00552.1
650 Eden C, Jung T (2001) North Atlantic interdecadal variability: oceanic response to the North Atlantic
651 Oscillation (1865–1997). J Clim 14: 676–691.
652 Feldstein SB (2003) The dynamics of NAO teleconnection pattern growth and decay. Q J R Meteorol Soc 129:
653 901-924.
654 Feser F, Barcikowska M, Krueger O, Schenk F, Weisse R, Xia L (2015) Storminess over the North Atlantic
655 and northwestern Europe-A review. Q J R Meteorol Soc 141: 350-382. doi: 10.1002/qj.2364
656 Fink AH, Pohle S, Pinto JG, Knippertz P (2012) Diagnosing the influence of diabatic processes on the
657 explosive deepening of extratropical cyclones. Geophys Res Lett 39: L07803. doi:10.1029/2012GL051025.
658 Fosdick EK, Smith PJ (1991) Latent Heat Release in an Extratropical Cyclone that Developed Explosively over
659 the Southeastern United States. Mon Wea Rev 119: 193-207.
660 Gilet JB, Plu M, Rivière G (2009) Nonlinear baroclinic dynamics of surface cyclones crossing a zonal jet. J
661 Atmos Sci 66: 3021-3041.
662 Gómara I, Pinto JG, Woollings T, Masato G, Zurita-Gotor P, Rodríguez-Fonseca B (2014a) Rossby Wave-
663 Breaking analysis of Explosive Cyclones in the Euro-Atlantic sector. Q J R Meteorol Soc 140: 738–753. .
664 doi: 10.1002/qj.2190

Gómara I, Rodríguez-Fonseca B, Zurita-Gotor P, Pinto JG (2014b) On the relation between explosive cyclones affecting Europe and the North Atlantic Oscillation. Geophys Res Lett 41: 2182-2190. doi:10.1002/2014GL059647.

Gyakum JR, Danielson RE (2000) Analysis of meteorological precursors to ordinary and explosive cyclogenesis in the western North Pacific. Mon Wea Rev 128: 851 - 863.

Hanley J, Caballero R (2012) The role of large-scale atmospheric flow and Rossby wave breaking in the evolution of extreme windstorms over Europe. Geophys Res Lett 39: L21708, doi:10.1029/2012GL053408

Hoerling MP, Hurrell JW, Xu T (2001) Tropical origin for recent North Atlantic climate change. Science 292: 90- 92

Hoerling MP, Hurrell JW, Xu T, Bates GT, Phillips A (2004) Twentieth century North Atlantic climate change. Part II: Understanding the effect of Indian Ocean warming. Clim Dyn 23: 391-405, doi:10.1007/s00382-004-0433-x

Honda M, Nakamura H, Ukita J, Kousaka I, Takeuchi K (2001) Interannual Seesaw between the Aleutian and Icelandic Lows. Part I: Seasonal Dependence and Life Cycle. J Climate 14: 1029-1042. doi: 10.1175/1520-0442(2001)014<1029:ISBTAA>2.0.CO;2

Hoskins BJ, McIntyre ME, Robertson AW (1985) On the use and significance of isentropic potential vorticity maps. Q J R Meteorol Soc 111: 877-946.

Hoskins BJ, Valdes PJ (1990) On the Existence of Storm-Tracks. J Atmos Sci 47: 1854-1864. doi: 10.1175/1520-0469(1990)047<1854:OTEOST>2.0.CO;2

Hoskins BJ, Hodges KI (2002) New perspectives on the Northern Hemisphere winter storm tracks. J. Atmos. Sci., 59 (6), 1041-1061.

Hurrell JW, Kushnir Y, Ottersen G, Visbeck M (2003) The North Atlantic Oscillation: climate significance and environmental impact. Geophys. Monogr. Series 134: 279pp.

James IN, James PM (1989) Ultra-low-frequency variability in a simple atmospheric circulation model. Nature 342: 53-55

Jung T, Hilmer M, Ruprecht E, Kleppek S, Gulev SK, Zolina O (2003) Characteristics of the Recent Eastward Shift of Interannual NAO variability. J Clim 16:3371-3382.

Jungclaus JH, Botzet M, Haak H, Keenlyside N, Luo JJ, Latif M, Marotzke J, Mikolajewicz U, Roeckner E (2006) Ocean circulation and tropical variability in the coupled model ECHAM5/MPI-OM. J Clim 19:3952-3972.

695 Kalnay E, and co-authors (1996) The NCEP/NCAR 40-Year Reanalysis Project, Bull the Am Meteorol Soc 77:
696 437-471.
697 Knight JR, Allan RJ, Folland CK, Vellinga M, Mann ME (2005) A signature of persistent natural thermohaline
698 circulation cycles in observed climate. Geophys Res Lett 32: L20708. doi:10.1029/2005GL024233.
699 Lau NC (1978) On the Three-Dimensional Structure of the Observed Transient Eddy Statistics of the Northern
700 Hemisphere Wintertime Circulation. J Atmos Sci 35: 1900–1923. doi: 10.1175/1520-
701 0469(1978)035<1900:OTTDSO>2.0.CO;2
702 Lau NC (1988) Variability of the Observed Midlatitude Storm Tracks in Relation to Low-Frequency Changes
703 in the Circulation Pattern. J Atmos Sci 45: 2718–2743. doi: http://dx.doi.org/10.1175/1520-
704 0469(1988)045<2718:VOTOMS>2.0.CO;2
705 Lee SS, Lee JY, Wang B, Ha KJ, Heo KY, Jin FF, Straus DM, Shukla J (2012) Interdecadal changes in the
706 storm track activity over the North Pacific and North Atlantic. Clim Dyn 39: 313-327. doi:
707 10.1007/s00382-011-1188-9
708 López-Parages J, Rodríguez-Fonseca B (2012) Multidecadal modulation of El Niño influence on the Euro-
709 Mediterranean rainfall. Geophys Res Lett 39: L02704. doi:10.1029/2011GL050049.
710 Losada T, Rodríguez-Fonseca B, Mechoso CR, Ma HY (2007) Impacts of SST anomalies on the North Atlantic
711 atmospheric circulation: a case study for the northern winter 1995/1996. Clim Dyn 29 (7-8): 807-819.
712 Losada T, Rodriguez-Fonseca B, Mohino E, Bader J, Janicot S, Mechoso CR (2012) Tropical SST and Sahel
713 rainfall: A non-stationary relationship. Geophys Res Lett 39: L12705 doi:10.1029/2012GL052423.
714 Lu J, Greatbatch RJ (2002) The changing relationship between the NAO and northern hemisphere climate
715 variability. Geophys Res Lett 29 (7) doi: 10.1029/2001GL014052.
716 Luksch U, Raible CC, Blender R, Fraedrich K (2005) Decadal Cyclone Track Variability in the North Atlantic.
717 Metorol Z special issue 14:747-753.
718 Marshall J, and coauthors (2001) North Atlantic climate variability: Phenomena, impacts and mechanisms. Int J
719 Climatol 21: 1863-1898.
720 Messori G, Caballero R (2015) On double Rossby wave breaking in the North Atlantic. J Geophys Res Atmos
721 120: 11,129-11,150. doi:10.1002/2015JD023854.
722 Minobe S, Kuwano-Yoshida A, Komori N, Xie SP, Small RJ (2008) Influence of the Gulf Stream on the
723 troposphere. Nature 452 (7184): 206–209

724 Mohino E, Janicot S, Bader J (2011) Sahel rainfall and decadal to multi-decadal sea surface temperature
725 variability. Climate Dynamics 37(3):419-440. DOI:10.1007/s00382-010-0867-2
726 Moore GWK, Renfrew IA, Pickart RS (2013) Multidecadal mobility of the North Atlantic Oscillation, J
727 Climate 26: 2453–2466.
728 Müller WA, Frankignoul C, Chouaib N (2008). Observed decadal tropical Pacific–North Atlantic
729 teleconnections. Geophys Res Lett 35: L24810. doi:10.1029/2008GL035901
730 Murray RJ, Simmonds I (1991) A numerical scheme for tracking cyclone centers from digital data. Part I:
731 development and operation of the scheme. Aust Meteor Mag 39: 155-166.
732 Nakamura H, Sampe T, Goto A, Ohfuchi W, Xie SP (2008) On the importance of mid-latitude oceanic frontal
733 zones for the mean state and dominant variability in the tropospheric circulation. Geophys Res Lett 35.
734 doi:10.1029/2008GL034,010
735 Nissen KM, Ulbrich U, Leckebusch GC, Kuhnel I (2014) Decadal windstorm activity in the North Atlantic-
736 European sector and its relationship to the meridional overturning circulation in an ensemble of simulations
737 with a coupled climate model. Clim Dyn 43(5-6): 1545-1555. doi:10.1007/s00382-013-1975-6
738 North GR, Bell TL, Cahalan RF, Moeng FJ (1982) Sampling errors in the estimation of empirical orthogonal
739 functions. Mon Wea Rev 110: 699-706. doi:10.1175/1520-0493(1982)110<0699:SEITEO> 2.0.CO;2
740 Osborn TJ, Briffa KR, Tett SFB, Jones PD, Trigo RM (1999) Evaluation of the North Atlantic oscillation as
741 simulated by a coupled climate model. Clim Dyn 15:685-702.
742 Petterssen S, Smebye SJ (1971) On the development of extratropical cyclones. Q J R Meteorol Soc 97: 457-
743 482. doi: 10.1002/qj.49709741407
744 Pinto JG, Spangehl T, Ulbrich U, Speth P (2005) Sensitivities of cyclone detection and tracking algorithm:
745 individual tracks and climatology. Meteorol Z 14: 823-838.
746 Pinto JG, Zacharias S, Fink AH, Leckebusch GC, Ulbrich U (2009) Factors contributing to the development of
747 extreme North Atlantic cyclones and their relationship with the NAO. Clim Dyn 32: 711-737.
748 Pinto JG, Reyers M, Ulbrich U (2011) The variable link between PNA and NAO in observations and in multi-
749 century CGCM simulations. Clim Dyn 36 (1-2): 337-354. doi: 10.1007/s00382-010-0770-x
750 Pinto JG, Raible CC (2012) Past and recent changes in the North Atlantic oscillation. Wiley Interdisciplinary
751 Reviews: Climate Change 3: 79-90. doi:10.1002/wcc.150

752 Pinto JG, Gómara I, Masato G, Dacre HF, Woollings T, Caballero R (2014) Large-scale dynamics associated
753 with clustering of extratropical cyclones affecting Western Europe. J Geophys Res Atmos 119, 13,704–
754 13,719, doi:10.1002/2014JD022305.
755 Raible CC, Luksch U, Fraedrich K, Voss R (2001) North Atlantic decadal regimes in a coupled GCM
756 simulation. Clim Dyn 18: 321-330
757 Raible CC, Luksch U, Fraedrich K (2004) Precipitation and Northern Hemisphere Regimes. Atmos Sci Lett 5:
758 43-55, DOI: 10.1016/j.atmoscilet.2003.12.001
759 Raible CC, Stocker TF, Yoshimori M, Renold M, Beyerle U, Casty C, Luterbacher J (2005) Northern
760 Hemispheric trends of pressure indices and atmospheric circulation patterns in observations,
761 reconstructions, and coupled GCM simulations. J Climate 18: 3968-3982
762 Raible CC, Della-Marta P, Schwierz C, Wernli H, Blender R (2008) Northern Hemisphere extratropical
763 cyclones: A comparison of detection and tracking methods and different reanalyses. Mon Wea Rev 136:
764 880-897.
765 Raible CC, Lehner F, Gonzalez-Rouco JF, Fernandez-Donado L (2014) Changing correlation structures of the
766 Northern Hemisphere atmospheric circulation from 1000 to 2100 AD, Climate of the Past 10: 537-550,
767 doi:10.5194/cp-10-537-2014.
768 Rayner NA, Parker DE, Horton EB, Folland CK, Alexander LV, Rowell DP, Kent EC, Kaplan A (2003) Global
769 analyses of sea surface temperature, sea ice, and night marine air temperature since the late nineteenth
770 century. J Geophys Res 108 (14): 4407. doi: 10.1029/2002JD002670
771 Reader MC, Moore GWK (1995) Stratosphere-troposphere interactions associated with a case of explosive
772 cyclogenesis in the Labrador Sea. Tellus A 47: 849-863.
773 Reichler T, Kim J, Manzini E, Kröger J (2012) A stratospheric connection to Atlantic climate variability.
774 Nature Geoscience 5: 783-787. doi:10.1038/ngeo1586.
775 Rivière G, Joly A (2006) Role of the low-frequency deformation field on the explosive growth of extratropical
776 cyclones at the jet exit. Part I: Barotropic critical region. J Atmos Sci 63: 1965-1981.
777 Rivière G, Gilet JG, Oruba L (2013) Understanding the Regeneration Stage Undergone by Surface Cyclones
778 Crossing a Midlatitude Jet in a Two-Layer Model. J Atmos Sci 70: 2832-2853.
779 doi: http://dx.doi.org/10.1175/JAS-D-12-0345.1
780 Rodríguez-Fonseca B, Polo I, Serrano E, Castro M (2006) Evaluation of the North Atlantic SST forcing on the
781 European and North African winter climate. Int J Climatol 26:179-191. DOI: 10.1002/7joc.1234

782 Rodríguez-Fonseca B, Polo I, García-Serrano J, Losada T, Mohino E, Mechoso CR, Kucharski F (2009) Are
783 Atlantic Niños enhancing Pacific ENSO events in recent decades? Geophys Res Lett 36: L20705.
784 doi:10.1029/2009GL040048.
785 Roeckner E, and coauthors (2003) The atmospheric general circulation model ECHAM 5. PART I: model
786 description. MPI Report 349.
787 Rogers JC (1997) North Atlantic Storm Track Variability and Its Association to the North Atlantic Oscillation
788 and Climate Variability of Northern Europe. J Climate 10 1635-1647. doi: 10.1175/1520-
789 0442(1997)010<1635:NASTVA>2.0.CO;2
790 Sanders F, Gyakum JR (1980) Synoptic-Dynamic climatology of the bomb. Mon Wea Rev 108: 1589-1606.
791 Sanders F (1986) Explosive cyclogenesis in the west-central North Atlantic Ocean. Part I: Composite structure
792 and mean behavior. Mon Wea Rev 114: 1781-1794.
793 Santos JA, Woollings T, Pinto JG (2013) Are the Winters 2010 and 2012 Archetypes Exhibiting Extreme
794 Opposite Behavior of the North Atlantic Jet Stream? Mon Wea Rev 141: 3626–3640. doi:
795 http://dx.doi.org/10.1175/MWR-D-13-00024.1.
796 Schneider EK, Bengtsson L, Hu ZZ (2003) Forcing of Northern Hemisphere climate trends. J Atmos Sci
797 60: 1504-1521
798 Seiler C, Zwiers FW (2015) How well do CMIP5 climate models reproduce explosive cyclones in the
799 extratropics of the Northern Hemisphere? Clim Dyn. doi: 10.1007/s00382-015-2642-x
800 Shapiro MA, Keyser D (1990) Extratropical Cyclones: The Erik Palmen memorial volume, chapter 10. Amer.
801 Meteorol. Soc.
802 Shindell DT, Schmidt GA, Mann ME, Rind D, Waple A (2001) Solar forcing of regional climate change during
803 the Maunder Minimum. Science 294: 2149-2152. doi:10.1126/science.1064363.
804 Stephenson DB, Pavan V, Bojariu R (2000) Is the North Atlantic Oscillation a random walk? Int J Climatol
805 20:1–18
806 Strong C, Magnusdottir G (2008) How Rossby wave breaking over the Pacific forces the North Atlantic
807 Oscillation. Geophys Res Lett 35: L10706. doi: 10.1029/2008GL033578.
808 Sun C, Li J, Jin F (2015) A delayed oscillator model for the quasi-periodic multidecadal variability of the
809 NAO. Clim Dyn 45: 2083–2099. doi: 10.1007/s00382-014-2459-z.

Sung MK, Ham YG, Kug JS, An SI (2013) An alterative effect by the tropical North Atlantic SST in intraseasonally varying El Nino teleconnection over the North Atlantic. Tellus A 65: 19863. doi: http://dx.doi.org/10.3402/tellusa.v65i0.19863

Trenberth KE (1997) The Definition of El Niño. Bull the Am Meteorol Soc 78: 2771-2777.

Trenberth KE, Branstator GW, Karoly D, Kumar A, Lau NC, Ropelewski C (1998) Progress during TOGA in understanding and modeling global teleconnections associated with tropical sea surface temperatures. J Geophys Res, 103(C7): 14,291–14,324. doi:10.1029/ 97JC01444.

Trigo IF (2006) Climatology and interannual variability of storm-tracks in the Euro-Atlantic sector: a comparison between ERA-40 and NCEP/NCAR reanalyses. Clim Dyn 26: 127-143.

Uccellini LW (1990) Processes contributing to the rapid development of extratropical cyclones. Extratropical Cyclones: The Erik Palmen Memorial Volume, C. Newton and E. O. Holopainen, Eds., American Meteorological Society, 81-105.

Ulbrich U, Christoph M (1999) A shift of the NAO and increasing storm track activity over Europe due to anthropogenic greenhouse gas forcing. Clim Dyn 15:551–559

Uppala SM, and co-authors (2005) The ERA-40 re-analysis. Q J R Meteorol Soc 131: 2961-3012.

Vicente-Serrano SM, López-Moreno JI (2008) Differences in the non-stationary influence of the North Atlantic Oscillation on European precipitation under different scenarios of greenhouse gas concentrations. Geophys Res Lett 35: L18710. doi:10.1029/2008GL034832.

Villamayor J, Mohino E (2015) Robust Sahel drought due to the Interdecadal Pacific Oscillation in CMIP5 simulations. Geophys Res Lett 42: 1214–1222. doi: 10.1002/2014GL062473.

Visbeck M, Cullen H, Krahmann G, Naik N (1998) An ocean model's response to North Atlantic Oscillation like wind forcing. Geophys Res Lett 25: 4521-4524.

Visbeck M, Chassignet E, Curry R, Delworth T, Dickson B, Krahmann G (2003) The Ocean's response to North Atlantic oscillation variability. In: Hurrell, J.W., Kushnir, Y., Ottersen, G., Visbeck, M. (Eds.), The North Atlantic Oscillation. AGU, pp. 113–146.

von Storch H, Zwiers F (1999) Statistical analysis in Climate research Cambridge University press, Cambridge

Wang C (2002) Atlantic Climate Variability and Its Associated Atmospheric Circulation Cells. J Climate 15: 1516-1536. doi: 10.1175/1520-0442(2002)015<1516:ACVAIA>2.0.CO;2

838 Wang C, Zhang L (2013) Multidecadal Ocean Temperature and Salinity Variability in the Tropical North
839 Atlantic: Linking with the AMO, AMOC, and Subtropical Cell. J Climate 26: 6137-6162. doi:
840 http://dx.doi.org/10.1175/JCLI-D-12-00721.1
841 Wang C, Zhang L, Lee SK, Wu L, Mechoso CR (2014) A global perspective on CMIP5 climate model biases.
842 Nature Climate Change 4: 201-205.
843 Wang YH, Magnusdottir G, Stern H, Tian X, Yu Y (2012) Decadal variability of the NAO: Introducing an
844 augmented NAO index. Geophys Res Lett 39: L21702. doi:10.1029/2012GL053413.
845 Wanner H, Bronnimann S, Casty C, Gyalistras D, Luterbacher J, Schmutz C, Stephenson DB, Xoplaki E
846 (2001) North Atlantic Oscillation-concepts and studies. Surv Geophys 22: 321-382.
847 Wernli H, Dirren S, Liniger MA, Zillig M (2002) Dynamical aspects of the life-cycle of the winter storm
848 "Lothar" (24–26 December 1999). Q J R Meteorol Soc 128: 405-429.
849 Woollings T, Hoskins B, Blackburn M, Berrisford P (2008) A New Rossby Wave-breaking Interpretation of
850 the North Atlantic Oscillation. J Atmos Sci 65: 609-626.
851 Woollings T, Hannachi A, Hoskins B (2010) Variability of the North Atlantic eddy-driven jet stream. Q J R
852 Meteorol Soc 136: 856-868. doi: 10.1002/qj.625
853 Woollings T, Gregory JM, Pinto JG, Reyers M, Brayshaw DJ (2012) Response of the North Atlantic storm
854 track to climate change shaped by ocean-atmosphere coupling. Nature Geoscience 5:313-317.
855 Woollings T, Franzke C, Hodson DLR, Dong B, Barnes EA, Raible CC, Pinto JG (2015) Contrasting
856 interannual and multi-decadal NAO variability. Clim Dyn 45:539-556. doi:10.1007/s00382-014-2237-y
857 Wunsch C (1999) The interpretation of short climate records, with comments on the North Atlantic and
858 Southern Oscillations. Bull Amer Meteor Soc 80: 245–255
859 Zappa G, Masato G, Shaffrey L, Woollings T, Hodges K (2014) Linking Northern Hemisphere blocking and
860 storm track biases in the CMIP5 climate models. Geophys Res Lett 41: 135-139.
861 doi:10.1002/2013GL058480.
862 Zhang L, Wang C (2013), Multidecadal North Atlantic sea surface temperature and Atlantic meridional
863 overturning circulation variability in CMIP5 historical simulations. J Geophys Res Oceans 118: 5772-
864 5791. doi:10.1002/jgrc.20390.
865 Zhang W, Wang L, Xiang B, Qi L, He J (2015) Impacts of two types of La Niña on the NAO during boreal
866 winter. Clim Dyn 44: 1351-1366.
867

Tables:

Table 1: Correlation coefficients between interannual cyclone track EOFs and climate indices in NCEP/ERA-40/ECHAM5

Corr.	NAO_T	AO	PNA	Niño-34	$Jet1_T$	$Jet2_T$
$All1_T$	**0.91/0.90/0.84**	**0.78/0.79/0.56**	-0.23/-0.23/**-0.17**	-0.15/-0.08/**-0.17**	**0.92/0.90/0.84**	-0.06/-0.12/**-0.16**
$EC1_T$	**0.78/0.88/0.66**	**0.63/0.74/0.38**	-0.16/-0.25/**-0.32**	-0.11/-0.27/**-0.13**	**0.72/0.85/0.59**	0.21/0.19/**0.29**
$All2_T$	0.08/0.10/**0.21**	-0.14/-0.18/**0.14**	0.04/-0.29/**0.17**	0.04/0.14/0.04	0.03/0.06/**0.15**	**0.55/0.55/0.36**
$EC2_T$	-0.12/-0.04/**-0.36**	**-0.26**/-0.21/**-0.19**	-0.05/**-0.44**/0.02	0.04/0.20/**0.17**	-0.22/-0.21/**-0.53**	**0.65/0.78/0.50**

Significant correlations (95%, t test) are shown with bold face. Cells are shaded when the correlation is significant for all datasets.

Table 2: Correlation coefficients between multi-decadal explosive cyclone track EOFs and low frequency (>11-yr) climate indices in ECHAM5/MPIOM1.

Corr.	NAO_{LF}	PNA_{LF}	AMO	IPO	AMOC	$Jet1_{LF}$	$Jet2_{LF}$
$EC1_{LF}$	**0.75**	-0.08	0.24	0.16	0.11	**0.68**	0.15
$EC2_{LF}$	-0.25	-0.01	-0.12	-0.09	-0.04	**-0.42**	**0.60**

Significant values (95%, t test) are shown with bold face and shaded cells.

879 **Figures**

880

881 **Fig. 1:** (a) Mean track density plots (in counts per 7.5° radius circle area per DJF season) of explosive
882 (contours) and non-explosive (shadings) cyclones based on NCEP (base period 1948-2011; all cyclone time
883 steps included). (b) EOF1 and explained variance (%) of DJF all cyclones (explosive + non-explosive)
884 anomalous track density fields ($ALL1_T$; shadings in track density units std^{-1} - 99% significance in stippling) and
885 u250 ($Jet1_T$; red/blue contours, starting from 2.5 in 0.5 intervals of m s^{-1} std^{-1}) based on NCEP. The
886 climatological jet stream core is shown in thick black contours (starting from 30 m s^{-1} with 5 m s^{-1} intervals). (c)
887 Same as (b) but for explosive track density fields only. (d) 21-yr running correlations (centered) of $EC1_T$ vs.
888 NAO_T (blue lines) and $EC1_T$ vs. $Jet1_T$ (red lines) for NCEP (solid lines) and ERA40 (dashed lines). All
889 correlations are significant (95% confidence interval, two sided t test). The magenta line is the AMO index.
890 1948-1962 and 1963-1997 periods denoted with black dashed and black solid horizontal lines.

891

892

893 **Fig. 2:** (a) Same as Fig. 1(c) but for the re-calculated EOFs for the base period 1948-1962. (b) Same as (a) but
894 for 1963-1997. (c) Regression (shadings, in gpm std^{-1}) and correlation (contours, 95% confidence interval) of
895 z500 winter anomalies on $EC1_{50s}$ (period 1948-1962). (d) Same as (c) but for $EC1_{80s}$ (base period 1963-1997).
896 (e) Re-calculated NAO pattern (NAO_{50s}; shadings in gpm std^{-1}, contours every 10 gpm std^{-1}) and explained
897 variance (in %) for the base period DJF 1948-1962. (f) Same as (e) but for 1963-1997 (NAO_{80s}). (g) Same as (c)
898 but for SST winter anomalies on $EC1_{50s}$ for the period 1948-1962 (in K std^{-1}; based on HadISST). (h) Same as
899 (g) but for $EC1_{80s}$ (base period 1963-1997).

900

901 **Fig. 3:** (a) Climatological winter zonal wind at 250 hPa (u250, contours in m s^{-1}) and 300-500 hPa maximum
902 Eady Growth rate (bi400, shadings in day^{-1}) on NCEP. (b) Difference of u250 intensity between 1948-1962 and
903 1963-1997 in red/blue shadings (m s^{-1}; 95% confidence interval marked with +). Difference of 300-500 hPa
904 Eady Growth rate (bi400) in contours (day^{-1}; 95% confidence interval marked with *x*). For the differences the
905 means of the second period are subtracted to the first one. (c) Low frequency (>33-yr.) u250 anomalies averaged
906 between 100°W-20°W in red/blue shadings (m s^{-1}). The thick black line follows the latitudinal location of the
907 maximum u250 positive anomalies. The thick dashed line is the decadal NAO index. Both indices are smoothed
908 (>33-yr low-pass filter), centered in the Y-axis and set to have the same standard deviation (the corresponding of

909 the jet latitude index) to allow comparison. (d) Same as (b) but for the winter SST in red/blue shadings (in K,
910 95% confidence interval in contours).
911
912 **Fig. 4:** (a) Same as Fig. 1(a) but for ECHAM5 (base period DJF 1-505 model years). (b) Difference in mean of
913 explosive track densities: ECHAM5 minus NCEP (shadings). Hatched areas depict significant differences (95%
914 confidence interval, t test for a difference in mean). (c) EOF1 and explained variance (%) of low-frequency
915 multi-decadal (>11-yr) DJF explosive anomalous track density fields ($EC1_{LF}$; shadings - 99% significance in
916 stippling) and u250 ($Jet1_{LF}$; red/blue contours, starting from 1 in 0.5 m s^{-1} std^{-1} intervals) on ECHAM5 (base
917 period DJF 1-505 years). (d) Same as Fig. 1(c) but for interannual timescales in ECHAM5 (1-11 yr.;
918 $EC1_T$/$Jet1_T$). (e) Regression (shadings, in gpm std^{-1}) and correlation (contours, 95% confidence interval) of z500
919 winter anomalies on interannual $EC1_T$ (1-11 yr.) for the total period of study on ECHAM5 (years 1-505). (f)
920 Same as (e) but for winter SST anomalies (K std^{-1}).
921
922 **Fig. 5:** (a) 21-yr running correlations (centered) of $EC1_T$ vs. NAO_T PCs (blue line) and $EC1_T$ vs. $Jet1_T$ PCs (red)
923 on ECHAM5. Significant values highlighted with thicker red/blue segments (95% confidence interval, two sided
924 t test). 'Decoupling periods' denoted with vertical bars. (b) *Magenta line:* Spatial correlation of NAO_T vs. the
925 485 running NAO patterns (based on 21-yr. sliding window EOFs). *Blue line:* Same as the magenta line but for
926 the 485 EC1 patterns vs. $EC1_T$. *Red line:* Latitudinal location (deg. N) of the main center of action of the 485
927 EC1 patterns (averaged over 90˚W-40˚E). (c) Same as Fig. 2(e) but for the decoupling periods on ECHAM5
928 (model years 182-209 and 305-327). (d) Same as Fig. 2(a) but for the decoupling periods on ECHAM5. (e)
929 Same as Fig. 2(c) but for the decoupling periods on ECHAM5. (f) Same as Fig. 2(g) but for the decoupling
930 periods on ECHAM5/MPIOM1.
931
932 **Fig. 6:** (a) Explosive track density anomaly for the decoupling periods (shadings; 95% confidence interval -
933 hatched) and standard deviation anomaly (contours; standard units, 95% confidence interval - filled dots). (b)
934 Climatological winter zonal wind at 250 hPa (u250, contours in m s^{-1}) and 300-500 hPa maximum Eady Growth
935 rate (bi400, shadings in day^{-1}) on ECHAM5. (c) Winter u250 anomaly (red/blue shadings in m s^{-1}, 95%
936 confidence interval marked with +) and 300-500 hPa Eady Growth rate anomaly (bi400, contours in day^{-1}, 95%
937 confidence interval marked with *x*) during the decoupling periods. (d) Same as Fig. 3(c) but for ECHAM5.
938 Decoupling periods marked with vertical bars.

Fig. 7: (a) Mean oceanic heat content (OHC) from 0 to 123 m (thermocline depth over the sub-tropical North Atlantic) in MPIOM1 (shadings in 10^9 J m^{-2}) and its meridional gradient (δyOHC) (contours in 10^9 J m^{-2} * 10^{-3} km). (b) Winter SST anomalies in shadings (K) and significant areas (95% confidence interval) in contours during the decoupling periods. Winter OHC significant anomalies (10^9 J m^{-2}) in stippling. (c) Meridional OHC gradient anomaly (δ_yOHC) (shadings in 10^9 J m^{-2} * 10^{-3} km) during the decoupling periods. Significant areas (95% confidence interval) in stippling. (d) Low pass filtered water temperature anomalies (>33 yr.; in SU) averaged over the area (30˚-40˚N, 60˚-30˚W, dashed rectangle in Fig. 7b) at different ocean depth levels (0, 6, 69 and 123 meters - see legend). Low pass filtered AMOC index (>33 yr.; dashed black curve in SU).

Fig. 8: (a) Schematic of the leading variability mode (1-11 yr.) of explosive cyclone tracks under normal conditions in ECHAM5/MPIOM1. EOF1 EC ($EC1_T$) in red shadings. Leading EOFs of u250 (1-11 yr.) in contours. These are the three preferred positions of the interannual jet (Woollings et al. 2010): (1) red - $Jet1_T$+/NAO+; (2) blue - $Jet1_T$-/NAO-; and (3) black - $Jet2_T$+. Main genesis area of explosive North Atlantic cyclones in stippling (values above 0.5 counts per 7.5^o radius circle area per DJF). (b) Same as (a) but for the decoupling periods.

Fig. 9: (a) Composite of DJF bi400 (shadings in day^{-1}) under NAO_T+ (>1 SU; 88 members). Base period: 1-505 yr. The areas of values above 40 day^{-1} are highlighted in stippling. (b) Same as (a) but under NAO_T- (<-1 SU; 88 members). (c) Same as (a) but under NAO_D+ (>1 SU; 8 members) during the decoupling periods. (d) Same as (a) but under NAO_D- (<-1 SU; 8 members) during the decoupling periods.

Fig. 10: Quantification of bi400 extent/strength over the North Atlantic: sum of all values in stippling from Figs. 9a-d associated with the extratropical jet (sub-tropical jet areas removed). The final values are normalized (in %) with respect to the climatological NAO_T+ absolute value (Fig. 9a).

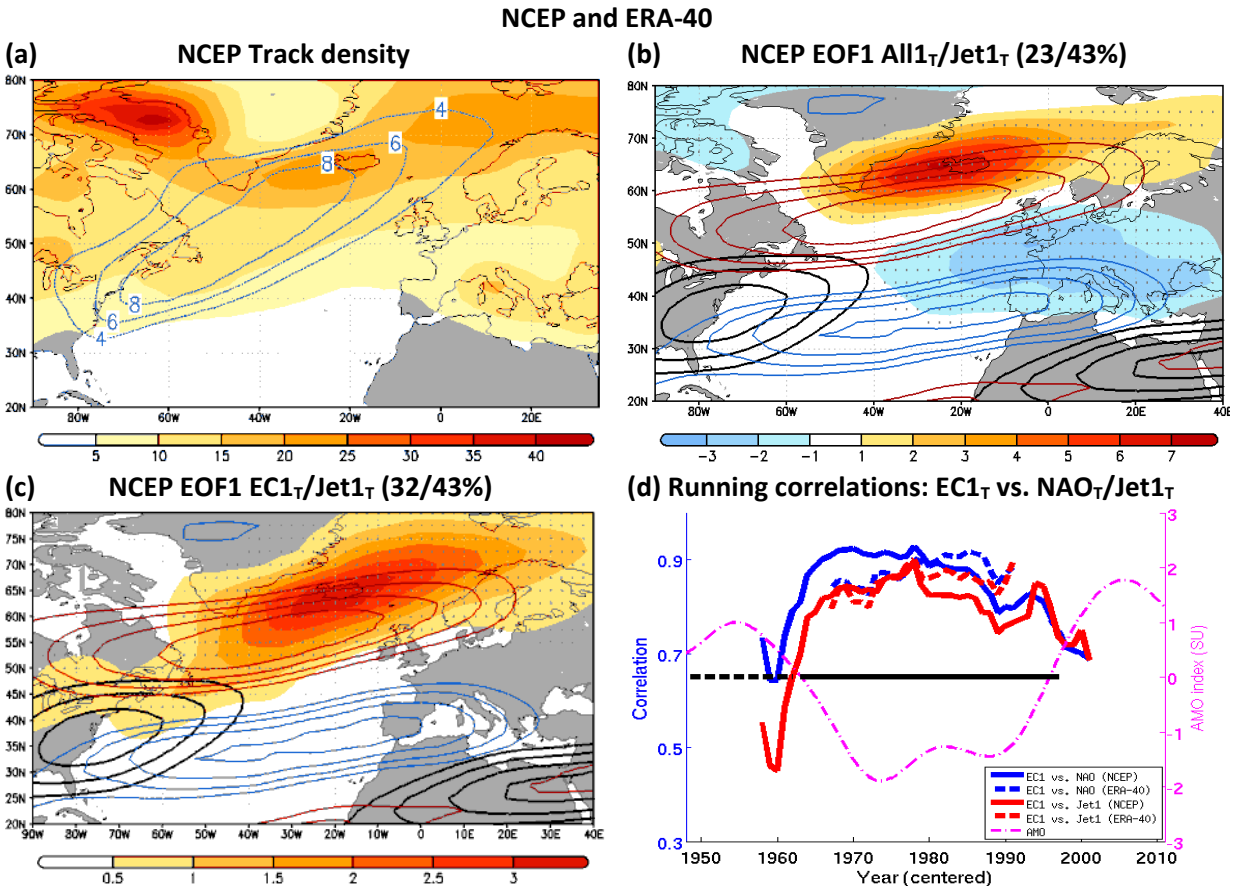
NCEP and ERA-40
(a) NCEP Track density
(b) NCEP EOF1 All1T/Jet1T (23/43%)
(c) NCEP EOF1 EC1T/Jet1T (32/43%)
(d) Running correlations: EC1T vs. NAOT/Jet1T
Correlation
AMO index (SU)
Year (centered)
EC1 vs. NAO (NCEP)
EC1 vs. NAO (ERA-40)
EC1 vs. Jet1 (NCEP)
EC1 vs. Jet1 (ERA-40)
AMO

964 **Fig. 1**

965

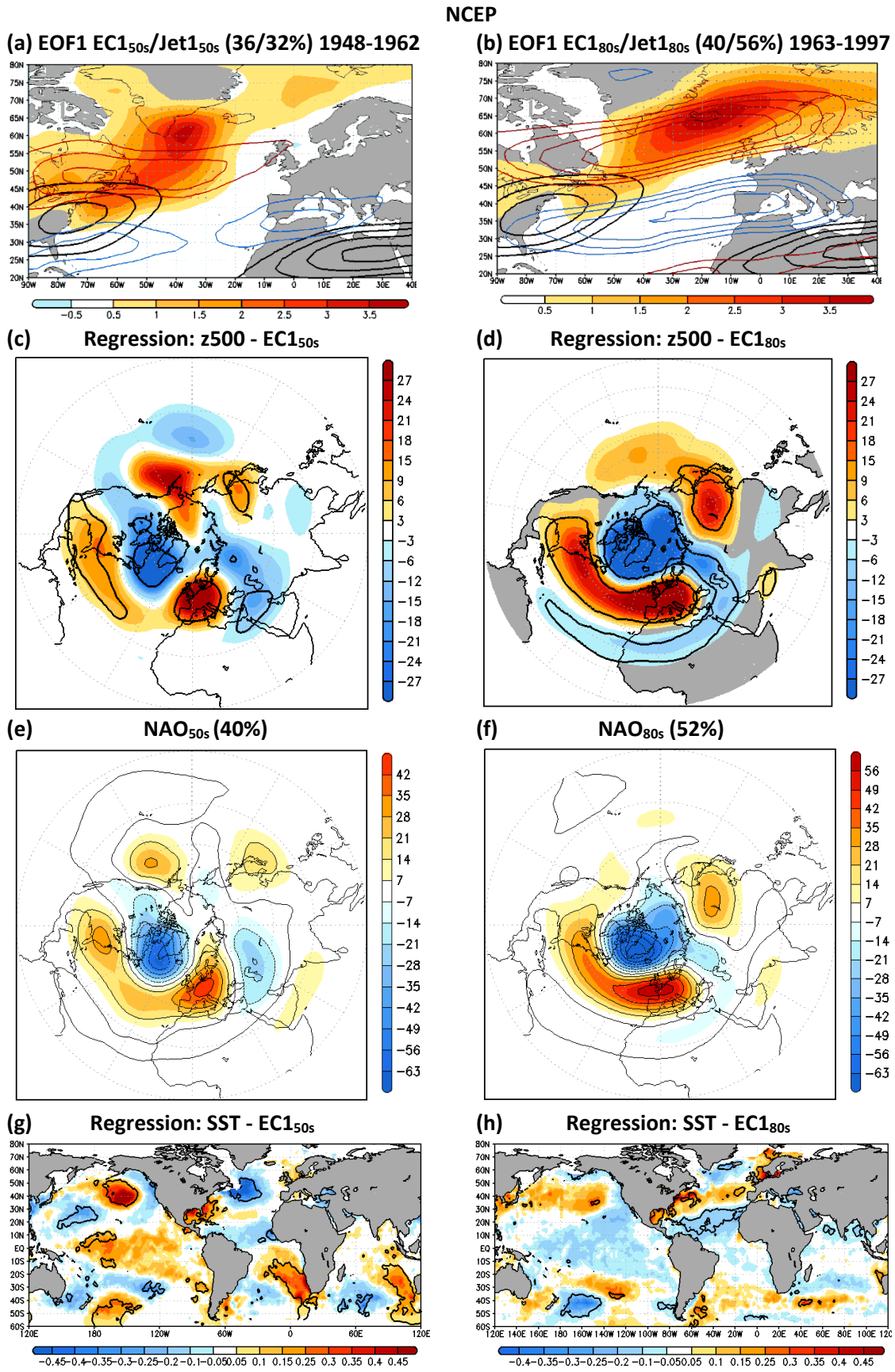
NCEP
(a) EOF1 EC1$_{50s}$/Jet1$_{50s}$ (36/32%) 1948-1962
(b) EOF1 EC1$_{80s}$/Jet1$_{80s}$ (40/56%) 1963-1997
(c) Regression: z500 - EC1$_{50s}$
(d) Regression: z500 - EC1$_{80s}$
(e) NAO$_{50s}$ (40%)
(f) NAO$_{80s}$ (52%)
(g) Regression: SST - EC1$_{50s}$
(h) Regression: SST - EC1$_{80s}$

966 **Fig. 2**

967

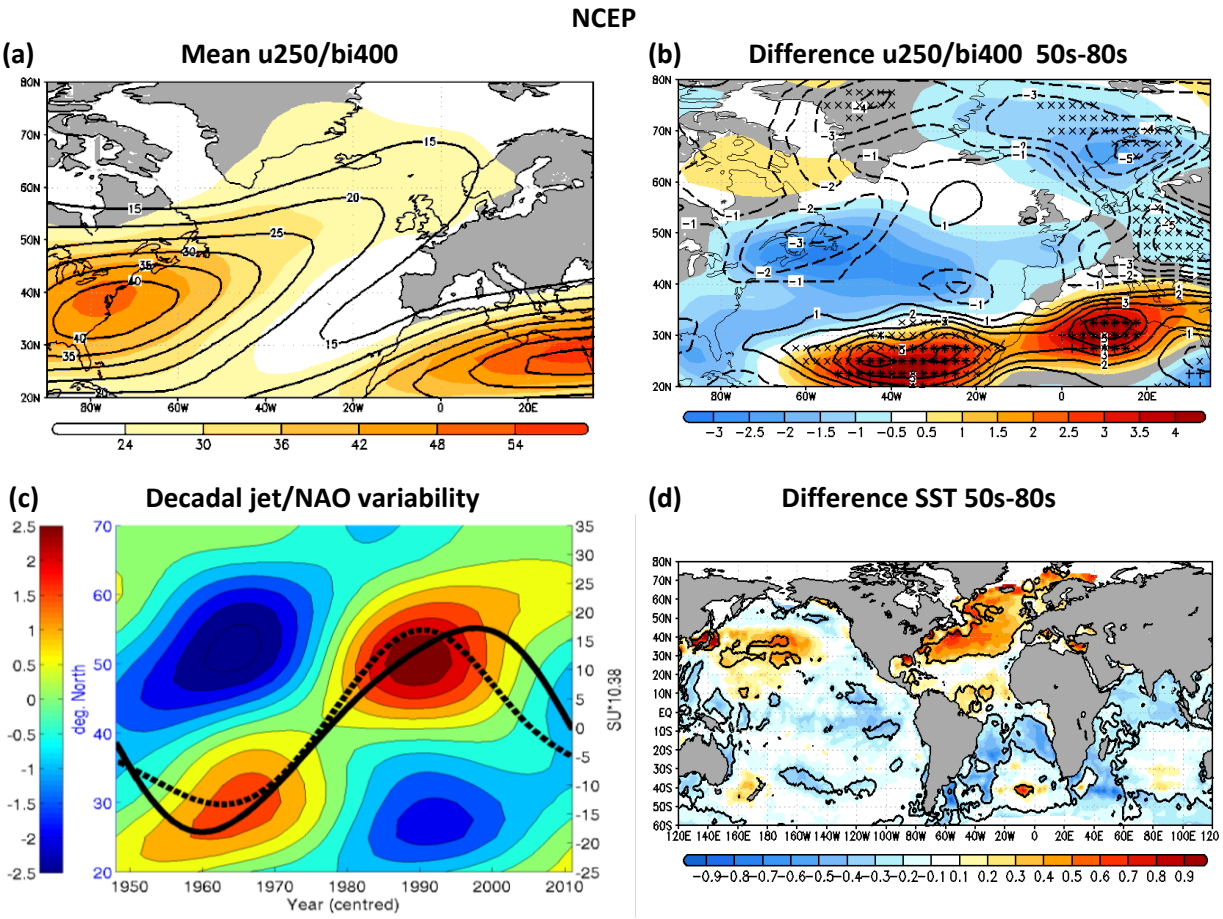

968 **Fig. 3**

969

970

971

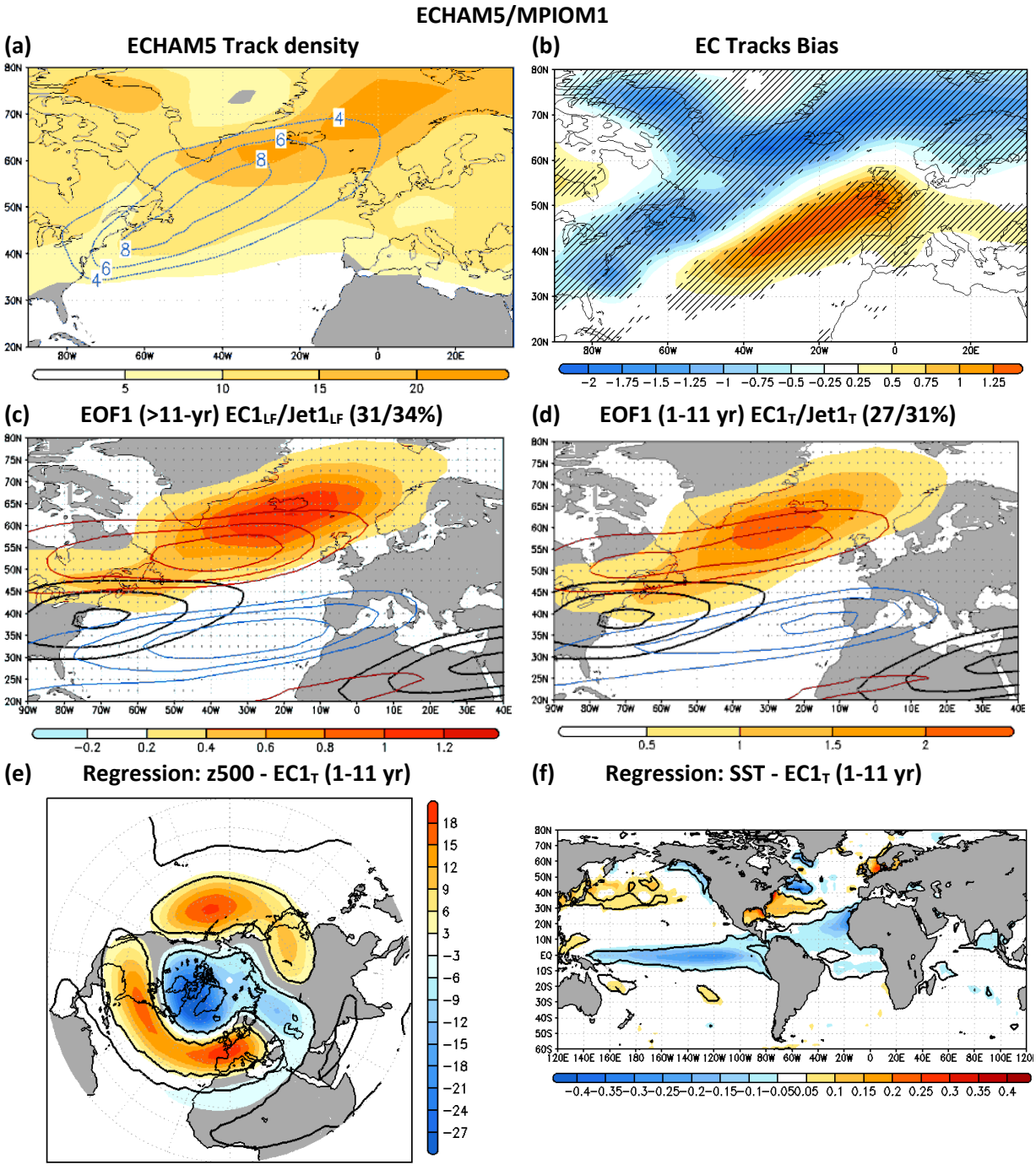
ECHAM5/MPIOM1
(a) ECHAM5 Track density
(b) EC Tracks Bias
(c) EOF1 (>11-yr) EC1LF/Jet1LF (31/34%)
(d) EOF1 (1-11 yr) EC1T/Jet1T (27/31%)
(e) Regression: z500 - EC1T (1-11 yr)
(f) Regression: SST - EC1T (1-11 yr)

Fig. 4

ECHAM5/MPIOM1

(a) Running correlations: $EC1_T$ vs. NAO_T/$Jet1_T$

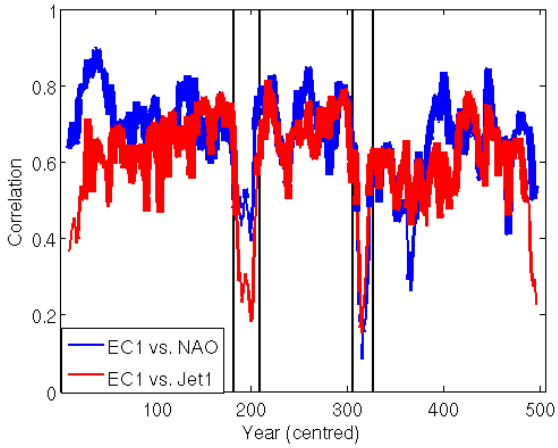

(b) Changes in the EOF patterns

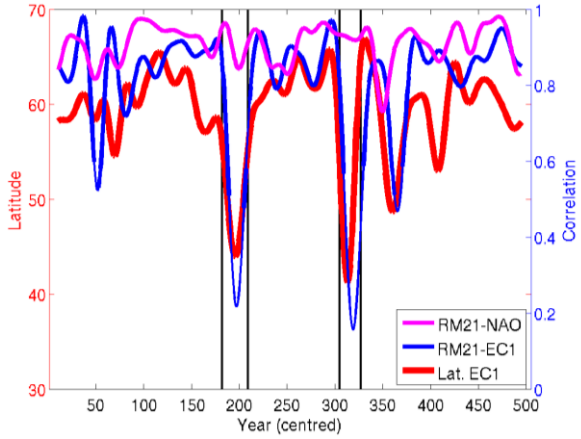

(c) Re-calculated NAO_D (40%)

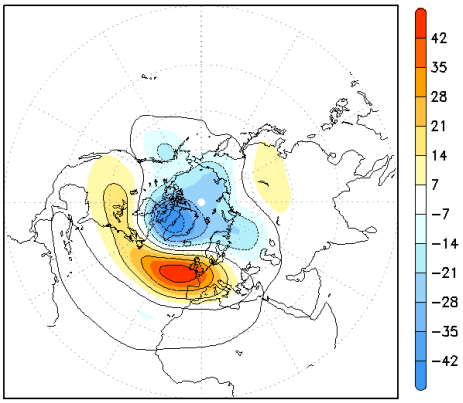

(d) $EC1_D$/$Jet1_D$ (26/36%): decoupling periods

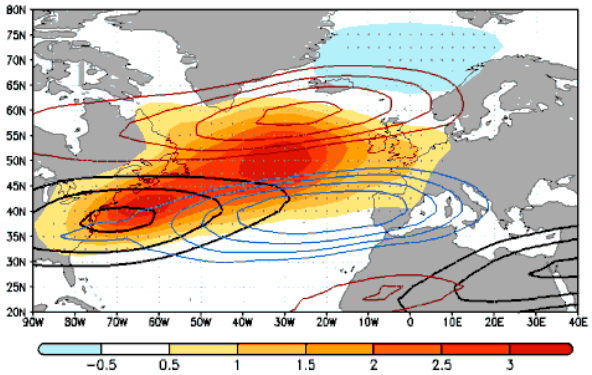

(e) Regression: z500 - $EC1_D$

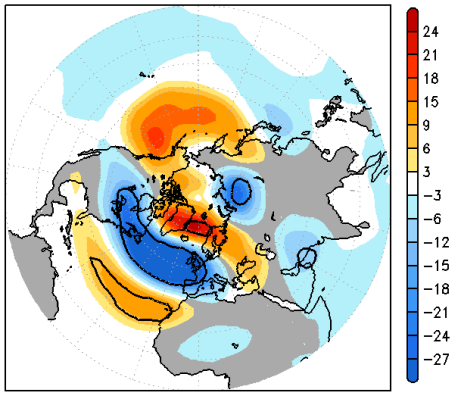

(f) Regression: SST - $EC1_D$

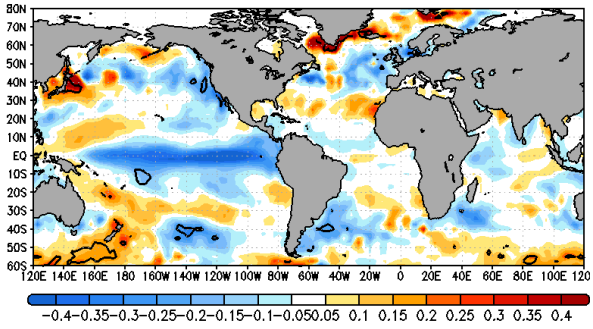

974 **Fig. 5**

975

976

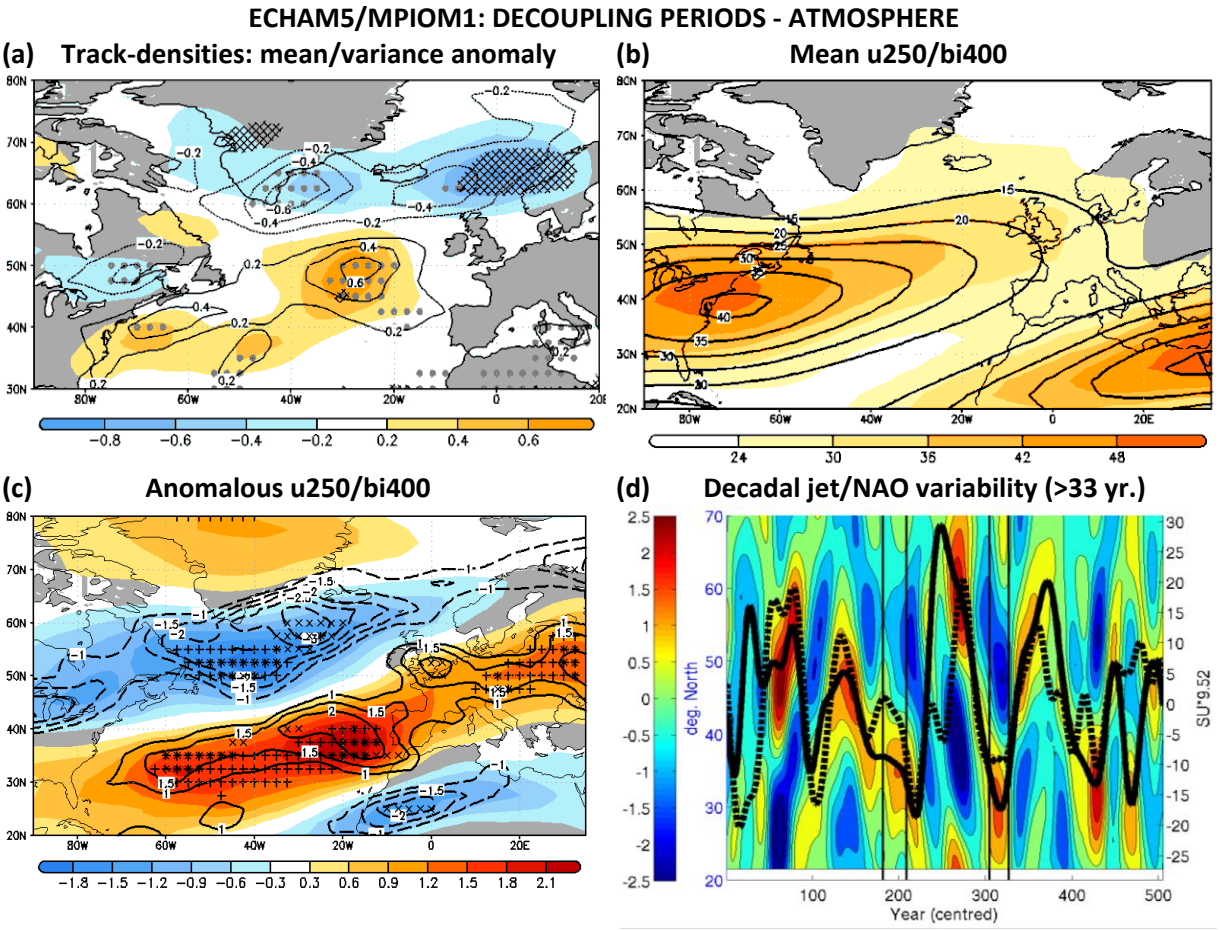
ECHAM5/MPIOM1: DECOUPLING PERIODS - ATMOSPHERE
(a) Track-densities: mean/variance anomaly
(b) Mean u250/bi400
(c) Anomalous u250/bi400
(d) Decadal jet/NAO variability (>33 yr.)
deg. North
SU*9.52
Year (centred)

977 **Fig. 6**

978

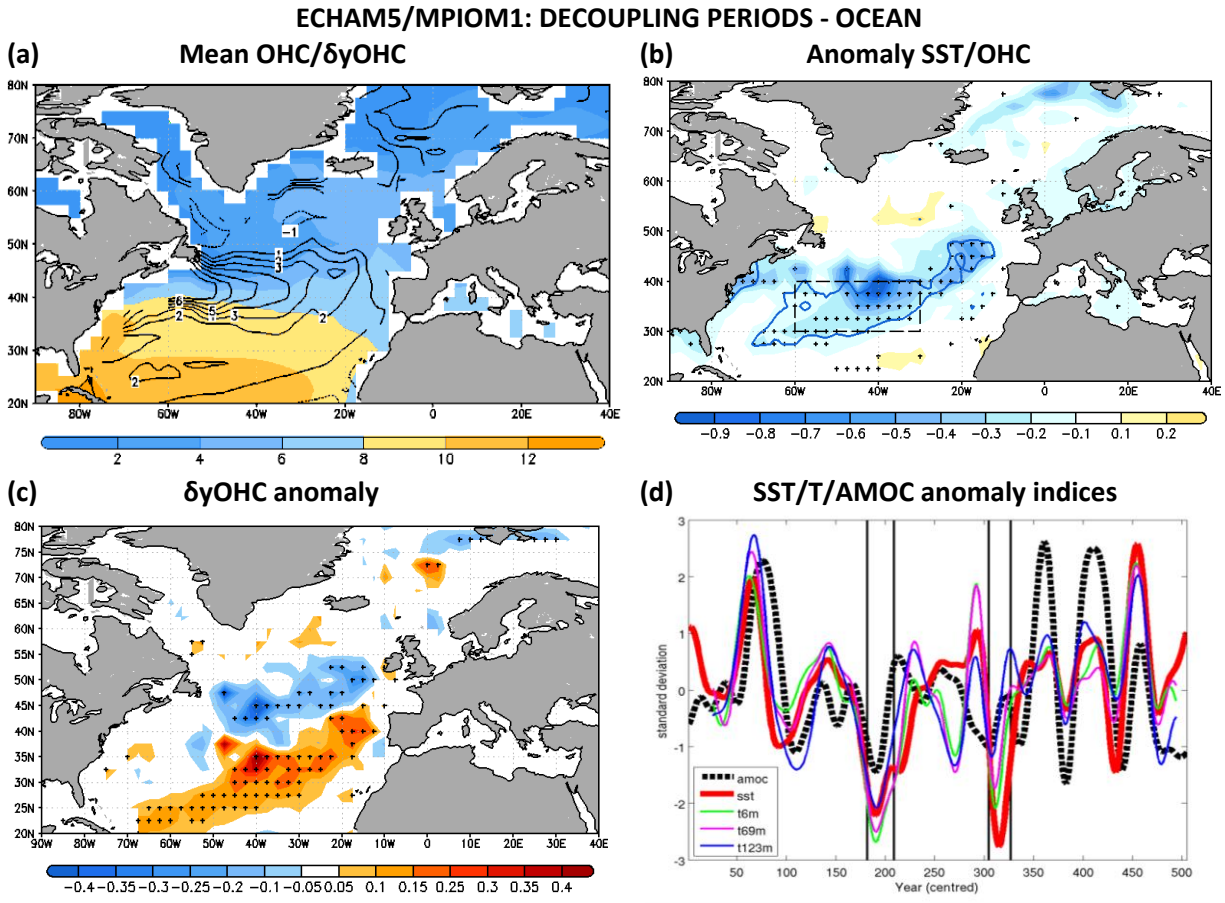
ECHAM5/MPIOM1: DECOUPLING PERIODS - OCEAN
(a) Mean OHC/δyOHC
(b) Anomaly SST/OHC
(c) δyOHC anomaly
(d) SST/T/AMOC anomaly indices
standard deviation
Year (centred)
amoc
sst
t6m
t69m
t123m

979 **Fig. 7**

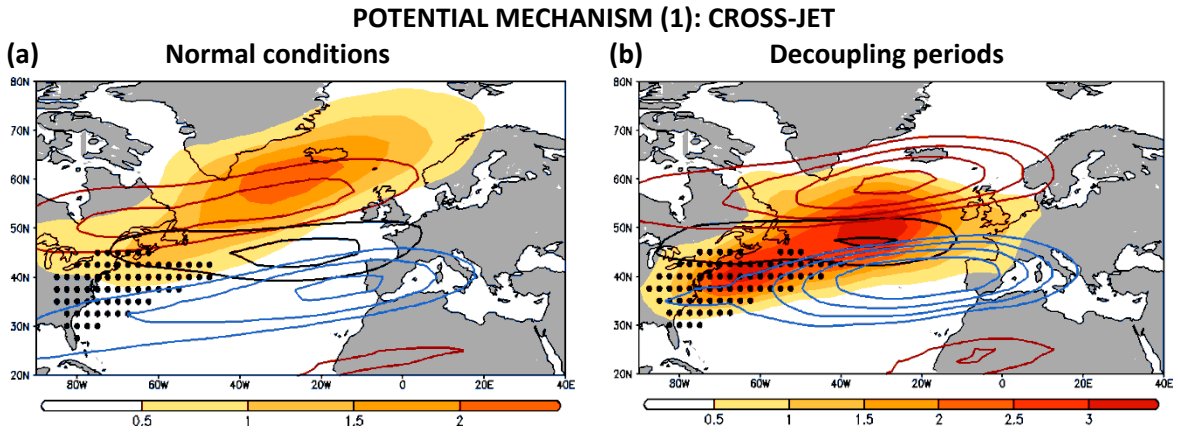
POTENTIAL MECHANISM (1): CROSS-JET
(a) Normal conditions
(b) Decoupling periods
80N
70N
60N
50N
40N
30N
20N
80W
60W
40W
20W
0
20E
40E
0.5
1
1.5
2
2.5
3

980 **Fig. 8**

981

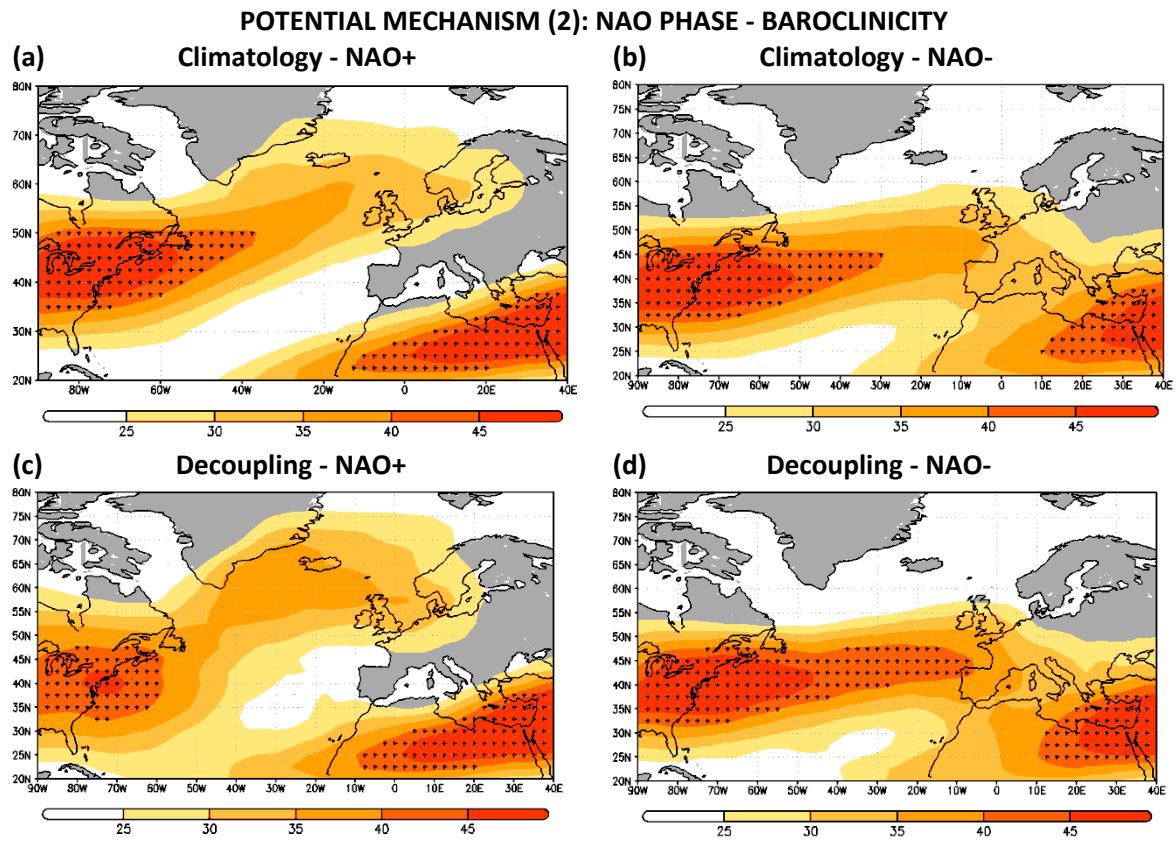
POTENTIAL MECHANISM (2): NAO PHASE - BAROCLINICITY
(a) Climatology - NAO+
(b) Climatology - NAO-
(c) Decoupling - NAO+
(d) Decoupling - NAO-
25
30
35
40
45

982 **Fig. 9**

983

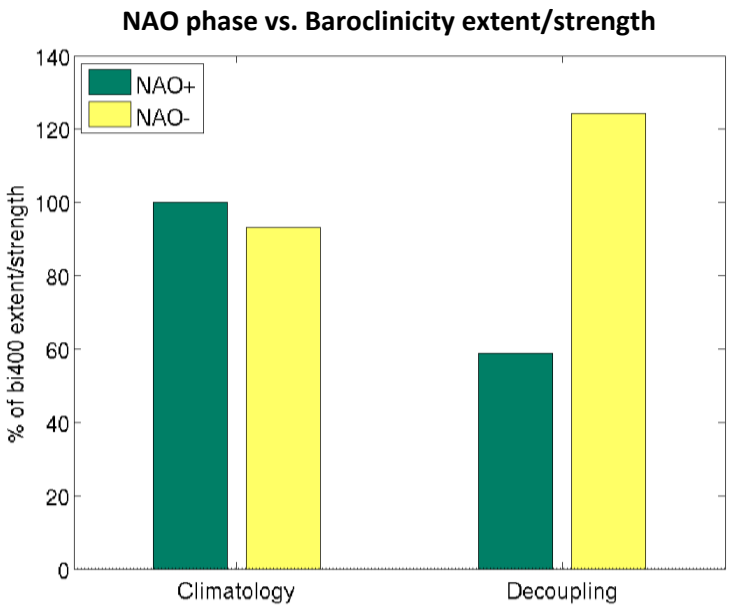
NAO phase vs. Baroclinicity extent/strength
NAO+
NAO-
% of bi400 extent/strength
0
20
40
60
80
100
120
140
Climatology
Decoupling

Fig. 10